Study of Heat Affected Zone of a weld in 9Cr-1.8W-0.5Mo Steel for Power Plant Application

A

Thesis

Submitted in partial fulfillment of requirements for the award of degree of

Masters of Technology

(Metallurgical and Materials Engineering)

by

S. Vinoth Kumar

(Reg. No.: 601302003)

Under the Supervision of

Dr. Kulvir Singh
Professor, SPMS
Thapar University, Patiala

Shri R. Ravibharath
Senior Development Engineer
WRI, BHEL-Trichy

School of Physics and Materials Science

Thapar University, Patiala-147004

July-2015

DECLARATION

I declare that this written submission represents my ideas in my own words and where other's ideas or words have been included, I have adequately cited and referenced the original sources. I also declare that I have adhered to all principles of academic honesty and integrity and have not misrepresented or fabricated or falsified any idea/data/fact/source in my submission. I understand that any violation of the above will be cause for disciplinary action by the Institute and can also evoke penal action from the sources which have thus not been properly cited or from whom proper permission has not been taken when needed.

S. Vinoth Kumar
Reg. No.: 601302003
School of Physics and Materials Science
Thapar University, Patiala

CERTIFICATE

This is to certify that the thesis entitled **"Study of Heat Affected Zone of a weld in 9Cr-1.8W-0.5Mo Steel for Power Plant Application"** which is being submitted by S. Vinoth Kumar (Reg. No. 601302003) in partial fulfilment of the requirements for the award of the degree of Master of Technology in Metallurgical and Materials Engineering from the School of Physics and Materials Science, Thapar University, Patiala (Punjab), India is an exclusive record of candidate's own research work under my guidance. The thesis in part or in full has not been submitted in any other university or institute for the award of any degree.

Dr. Kulvir Singh
Professor, School of Physics and Materials Science
Associate Dean, Strategy
Thapar University
Patiala-147004 (INDIA)

Countersigned by

Dr. Manoj Sharma
Professor and Head
School of Physics and Materials Science
Thapar University
Patiala-147004 (INDIA)

Dr. S.S Bhatia
Dean of Academic Affairs
Thapar University
Patiala-147004 (INDIA)

BHARAT HEAVY ELECTRICALS LIMITED
WELDING RESEARCH INSTITUTE,
TIRUCHIRAPPALLI-620 014, INDIA

R.Ravibharath
Deputy Manager

American Welding Society
Educational Institution Member

Ref. No. RRB/07/05 **Date: July 20, 2015**

PROJECT COMPLETION CERTIFICATE

This is to certify that **Mr. S. Vinoth Kumar, (M.Tech. Metallurgical and Materials Engineering Reg. No.: 601302003),** a student of Thapar University, Patiala has carried out his M.Tech Dissertation work titled "**Heat Affected Zone Simulation and Characterization of Grade 92 (9Cr-1.8W-0.5Mo) Steel TIG weldment**" at Welding Research Institute in Bharat Heavy Electricals Limited, Tiruchirappali. During this tenure his conduct was satisfactory.

R. Ravibharath
(6125603)
Deputy Manager,
Welding Research Institute
Bharat Heavy Electricals Limited
Tiruchirappalli-620015

ACKNOWLEDGEMENTS

I express my profound gratitude to my project guide **Dr. Kulvir Singh,** Professor, School of Physics and Materials Science, Thapar University, Patiala for his valuable guidance, motivation and the keen interest he had taken throughout the course of this project work.

I am also extremely thankful to **Shri R. Ravibharath,** Senior Development Engineer Welding Research Institute, BHEL, Trichy, for providing valuable guidance and giving me an opportunity to complete this project successfully.

I am also thankful to **Shri R. Easwaran,** General Manager, Welding Research Institute, BHEL, Trichy, consent to me to do the project and for the valuable guidance.

I sincerely thank **Dr. Manoj Sharma,** Professor and Head, School of Physics and Materials Science, Thapar University, Patiala for permitting me to carry out this project of research relevance in the department with comfort.

I would like to thank **Shri P. Mourgane,** Assistant Engineer, Welding Research Institute, BHEL, Trichy, for support during entire period of my project.

I am also very much thankful to **Shri Senthil Kumar, Shri Ramajeyam Murugan, Shri Rengan** and **Shri Marappan**, Welding Metallurgy Department, Welding Research Institute, BHEL, Trichy, for their constant support and who were always at hand to help at every junction.

I personally thank **Mohankumar, Prabhakaran, Arokia Stephan Raj, Prathap Singh, Ram Prasad**, and **Dhanapal**, Apprentice trainees who were always ready to help in all regards.

I also thank to all faculty members and other staff members of School of Physics and Materials Science, Thapar University, Patiala for all the support during the course of period.

Last but not least, I recall the continuous support and encouragement rendered by my best friends and my family members which led to the successful completion of this project.

(S. Vinoth Kumar)

INDEX

Content	***Page No.***
Certificate	ii
Acknowledgement	vi
List of figures	viii
List of tables	ix
Abstract	xi
Chapter - 1	
Introduction and literature review	
1.1 Steel for power plant	1
1.2 Literature review	3
1.2.1 ASTM A 335 grade P92	3
1.2.2 Physical metallurgy of P92	4
1.2.3 Precipitates in power plant steels	5
1.2.3.1 MX	6
1.2.3.2 $M_{23}C_6$	6
1.2.3.3 Laves Phase	6
1.2.3.4 Z-Phase	6
1.2.4 Continuous Cooling Transformation (CCT)	6
1.2.5 Advantages of P92	7
1.2.6 Application of P92 steel	8
1.2.6.1 Boiler engineering	8
1.2.6.2 Nuclear power plants	8
1.2.6.3 Petrochemical plants	9
1.2.7 Weldability of P92	9
1.2.7.1 Welding and welding consumables for Cr-Mo steels	9
1.2.8 Heat treatments for Cr-Mo steels and welded joints	12

1.2.9 Heat affected zone (HAZ) subzones 13

1.2.10 Crack types in steel weldments 14

1.2.10.1 Type-I & II crack 14

1.2.10.2 Type-III crack (reheat crack) 14

1.2.10.3 Type-IV crack 15

1.2.11 Sysweld

1.2.12 Physical / thermo-mechanical simulation 21

Chapter - 2

Experimental Procedures

2.1 GTAW welding of P92 23

2.1.1 Edge preparation 23

2.1.2 Preheat 24

2.1.3 Post-weld heat treatment (PWHT) 24

2.2 Welding parameters (trial) 25

2.2.1 Optimised weld parameters 26

2.3 Sample preparation for weld evaluation 26

2.3.1 Optical microscopy for macro and microstructures 26

2.3.2 Mechanical testing of weld 27

2.3.2.1 Micro-hardness test 27

2.3.2.2 Tensile test 27

2.3.2.3 Bend test 28

2.3.2.4 Impact test 28

2.4 Sysweld-FEM 28

2.5 Physical simulation-thermo mechanical simulator 30

2.5.1 Effect of free span 32

2.5.2 Grips 33

2.5.3 HAZ simulation 33

2.5.4 Quicksim 33

2.5.5 Specimen preparation 34

Chapter - 3

Results and Discussion

3.1 Macrostructural analysis of weld 35

3.2 Weldment analysis 36

3.2.1 Microstructure analysis 36

3.2.2 Micro-hardness analysis 37

3.2.3 Weld toughness analysis 37

3.2.4 Tensile test analysis 38

3.2.5 Bend test analysis 39

3.3 Sysweld simulation analysis 39

3.4 Heat affected zone analysis 41

3.4.1 HAZ micro-hardness correlation 43

3.4.2 Thermal cycle and microstructure comparison 44

3.4.3 Fracture toughness 56

Chapter - 4

Conclusion and Future scope

4.1 Conclusion 58

4.2 Future scope 59

References 60

List of Figures

Chapter – 1 ***Page No.***

Figure 1.1 Dilation and CCT of P92 7

Figure 1.2 Heating cycle for weld 12

Figure 1.3 Subzones of HAZ after welding 14

Figure 1.4 Types of crack in weld joints of steel on service exposure 16

Figure 1.5 (a) Lath martensitic structure in modified 9Cr-1Mo base metal 18
(b) Recovered subgrain structure in inter-critical HAZ 18
(c) Z-Phase in the inter-critical HAZ. 18

Figure 1.6 Double ellipsoidal heat source 20

Chapter – 2

Figure 2.1 Edge preparation 24

Figure 2.2 Reduced rectangular section tension specimens for pipe 27

Figure 2.3 Charpy test subsize specimen 28

Figure 2.4 Gleeble® 3800 thermo mechanical simulator and simulating sample 31

Figure 2.5 Temperature distributions along the specimen at different free span 32

Figure 2.6 Water-cooled copper grip contribute to very fast cooling rates and enable to simulate steep thermal gradients found in welding applications 33

Chapter – 3

Figure 3.1 Transverse view of welded specimen macrostructure 35

Figure 3.2 Microstructure of weld 36

Figure 3.3 Hardness profile comparison 37

Figure 3.4 Brittle fracture of weld Metal 38

Figure 3.5 Tensile test Specimen 39

Figure 3.6 Bend test macrostructure 39

Figure 3.7 Sysweld simulation of weld thermal cycle 40

Figure 3.8 Hardness comparison for simulated and real time HAZs 43

Figure 3.9 Region 1 to 11- Simulated weld thermal cycle and microstructure 49

1. Top-1.067 mm (690/1204 °C) 44
2. Top-0.652 mm (652/1089 °C) 45
3. Top-0.812 mm (612/970 °C) 46
4. Top-0.89 mm (567/872 °C) 47
5. Middle-0.88 mm (957/1330 °C) 48
6. Middle-1 mm (718/1122 °C) 49
7. Middle-2.4 mm (662/1013 °C) 50
8. Bottom-0.64 mm along fusion line (1362/1310 °C) 51
9. Bottom-(0.45,0.85 mm) (1265/1293 °C) 52
10. Bottom-(1.42, 1.01 mm) (1060/1229 °C) 53
11. Bottom-(1.02, 1.14 mm) (878/1148 °C) 54

Figure 3.10 Shear fracture of simulated samples-Peak temperature of 1060/1229 °C 57

Figure 3.11 Brittle fracture of simulated samples-Peak temperature of 957/1330 °C 57

List of Tables

Chapter – 1 ***Page No.***

Table 1.1 Chemical Composition of P92 according to ASME Sec II Part A 4

Table 1.2 Precipitations in creep resistant Cr-Mo steels 5

Table 1.3 Welding consumable for Cr-Mo steels 10

Table 1.4 HAZ subzones and its characteristics 13

Table 1.5 Classification of cracks in steel welds 17

Chapter - 2

Table 2.1 Welding trail 25

Table 2.2 Optimised parameters 26

Table 2.3 Temperature dependent physical properties of P92 29

Table 2.4 Temperature dependent mechanical properties of P92 30

Chapter - 3

Table 3.1 Tensile test result 38

Table 3.2 Comparison of HAZs 41

Table 3.3 Peak temperatures and hardness comparison chart 42

ABSTRACT

Continuous improvement in steam parameters for achieving higher efficiencies led to the development of many new creep resistant steels in thermal power plant industry. As welding is the major fabrication technique used in power plant construction, these creep resistant steel should possess good weldability and in-service life condition.

This thesis contains a presentation of basic problems appears in service at Heat Affected Zones (HAZs) of membrane panels and high temperature pipe lines made of tempered bainitic/martensitic creep resistant 9Cr-1.8W-0.5Mo (Grade 92) steel used for boilers operating at supercritical parameters. The HAZs of these components often experience Type-IV creep crack due to micro-coalescence of creep voids at operating temperature.

Welding thermal cycles had been simulated with Finite Element Simulation using SYSWELD and with these thermal cycles physically HAZs had been simulated and studied for its microstructure, hardness and toughness in-situ comparison with real time HAZ during welding. The experimental results will be used to study the creep failure to develop a further modification in the parent metal, which can serve as a bench mark for the future development of creep strength enhanced steels.

Chapter – 1

Introduction and Literature Review

1.1 Steel for Power Plant

The increase in world population led to the demand of increasing electrical power supply across the world. Researches have been going all around the world to eliminate the electrical power crisis which is supposed to happen in the near future. This led to the development of new materials and technology which will increase the efficiency of currently operating fossil fuel power plant which will be the major candidate for power supply as other technologies like nuclear and solar have their own drawbacks. The challenge facing today is to develop a technology that produces electrical energy with maximum efficiency and minimum environmental damage. In typical fossil fuelled plant, higher operating efficiencies can only be achieved by escalating the pressure and temperature of the steam.

Candidate materials have been considered, such as high chromium ferritic/martensitic (F/M) steels, austenitic stainless steels, SiC/SiC composite, vanadium base alloys, reduced activation F/M (RAFM) steels and oxide dispersion strengthen (ODS) steel. As per the projected demand of power companies, these materials were formed to raise power efficiency, which is to burn a smaller amount of fossil fuel to higher temperatures. These materials can overcome operational costs and meet up the stringent ecological desires. These improvements of thermal efficacy in power production by escalating the operational temperature (600 °C) and pressure (170-230 bar) has freshly steer to the improvement of new kin of heat resistant steels. The use of creep resisting alloy steels like modified 9Cr-1Mo (grade 91) developed in USA by ORNL (Oak Ridge National Laboratory) around late 80's made remarkable development in improving operating efficiencies of thermal power plants. But demand for increasing operating efficiencies leads to development of new materials with enhanced creep properties like grade 92 than the earlier available creep resisting steels. Grade 92 is a modification of grade 91 with the addition of 2% tungsten replacing most of the molybdenum. Micro alloying with up to 0.006% (60 ppm) boron increases the creep resistance. Grade 92 is primarily considered as a piping material for high steam conditions and is seen as a great enhancement on P9 series, with an advantage of rupture strength of about 30% at 600 °C.

According to the American Society for Mechanical Engineers (ASME), boiler and pressure vessel code, Section – 1 and 9, CSEF steels (Creep Strength Enhanced Ferritic steels) are a group of ferritic steels where its creep strength was improved by the formation of martensitic/bainitic microstructure that become stable at tempering by forced precipitation of carbo-nitrides, temper resistant carbides etc. More recent developments in CrMo alloy steel grades like P91, P92 and P122 have enhanced mechanical properties at elevated temperatures, in particular, rise in creep strength of 30% at 100,000 h in 600 °C for P92. This made it feasible to decrease the wall width of the pipes and accordingly develop their performance to thermal fatigue. As welding is the major fabrication technique used in thermal power plant construction, it is required that steels used in construction should possess good weldability, while creep resistant ferritic steels are joined effectively by all widespread welding methods like Gas Tungsten Arc Welding (GTAW), Shielded Metal Arc Welding (SMAW), Submerged Arc Welding (SAW) covering a wide range of thickness that are suitable for power plant service, HAZ of weld in this steels are susceptible to crack such as Type-IV i.e. premature creep failure in the fine grained / inter-critical heat affected zone. As in-depth understanding of HAZ is critical due to large thermal gradient for successful induction of this P92 alloy in power plants, hence in this current work the resultant HAZ of GTAW welding process and after Post Weld Heat Treatment (PWHT) process has been passed out and compared with enlarged HAZ's samples with consistent temperature region were produced by physical simulator Gleeble® 3800, with the support of SYSWELD - Finite Element Analysis (FEA). These weld and simulated HAZ's were characterized using optical Microscope, Hardness test, Tensile test, and impact test and also used for characterizing the weld [1, 2].

The thermo-mechanical processing and treatment play a pivotal role in the design and development of high performance steels. Therefore, physical process simulation becomes a necessary tool for better microstructural understanding and useful predictions of ensuing process-structure-properties correlation.

1.2 Literature Survey

Thermal power plants generate electrical energy by flaming coal in boiler where water converted to steam having higher temperature and pressure. This steam flows through a series of pipes and fall on turbines which steer an electrical generator to generate voltage difference. The condensation of drain out vapour from turbine is returned back to boiler to repetition. For achieving maximum output efficiencies, the temperature and pressure of steam should be continuously increased for achieving super critical parameters. The steam parameters in super critical power plants are continually growing which requires new superior materials with improved creep potency to operate at high temperatures. Efficient power plants require material properties like improved creep strength, superior corrosion and hot corrosion degradation stability. The final super heater tubes, economizer tubes and membrane water wall (MWW) tubes must provide improved high temperature strength. The final super heater tubes, economizer tubes and membrane water wall (MWW) tubes must provide improved high temperature strength. Conventional T/P91 (9Cr-1Mo) is not meeting the specified strength of creep for using it as water walls panels for Ultra super critical boilers. This led to development of grade 92 steels.

1.2.1 ASTM A 335 Grade P92

Grade P92 is a ferritic/martensitic steel, microalloyed with vanadium, niobium and controlled boron and nitrogen content which then normalized at 1040-1080 °C and tempered at 760 °C to have martensitic or bainitic microstructure with precise precipitation of temper resistant carbides and carbo-nitrides which was originally developed by Nippon Steel in the name of NF616 as an alternative to Grade P91. Advantages of the P92 are high temperature strength and creep behavior, corrosion-oxidation resistance equal to other 9%Cr ferritic alloy steels. To understand the ferritic/martensitic formation, we have to study physical metallurgy and continuous cooling transformation [3].

1.2.2 Physical Metallurgy of P92

These steels are strengthened and resisted towards corrosion by introducing alloy elements into the matrix which are shown in table 1.1 and illustrated below [4].

Table 1.1 P92 Chemical compositions according to ASME Sec. II Part A.

Grade	%	C	W	Mn	P	S	Si	Cr	Mo	V	Nb	N	B	Al	Ni
T/P92	Min.	0.07	1.5	0.3	-	-	-	8.5	0.3	0.15	0.04	0.03	0.001	-	-
	Max.	0.13	2.0	0.6	0.02	0.01	0.50	9.5	0.6	0.25	0.09	0.07	0.006	0.04	0.40

1. Carbon and Nitrogen are strong austenite stabilizers and have limited solubility in ferrite so they precipitate out leading to formation of carbides and nitrides. Carbon content increases $M_{23}C_6$ to a great extent where as nitrogen increases, Z-phase also increase.
2. Mo and W are important constituent of laves phase and are good ferrite stabilizing elements. An increase in either of the two will increase the fraction of laves phase but Z-phase remains unaffected. Mo is strong ferrite stabilizer than W so some extent of W is added instead of Mo to increase the strength and also creep strength where high W also leads to detrimental lower delta ferrite.
3. Cr is primarily added to increase high temperature oxidation and corrosion resistance. Increase in Cr leads to increase in Laves phase and also facilitates Z-phase precipitation.
4. V and Nb are carbide and nitride formers and are important for MX precipitation (M-Metal atoms, X-C, N). Niobium carbides are very stable and remain undissolved even during austenization. Increase in their content seems to increase the MX precipitates in matrix but also increase the Z-Phase formation.
5. Boron is added as a surface or grain boundary active element which will hinder the coarsening of $M_{23}C_6$ precipitates by segregating along the grain boundaries thus increasing the creep strength of the steel.
6. Cu has low solubility in steels and increase the toughness of the steel but leads to failure by precipitating along the sub-grain boundaries and act as nucleation site for crack initiation.

1.2.3 Precipitates in Power Plant Steels

High creep strength of P92 steel is induced by elements W and Mo and precipitates as $M_{23}C_6$ carbides and fine precipitates of carbo-nitrides (especially the MX phase of the carbo-nitrides). Its importance is that in mid of these fortifying additives, in general the outcome of MX phase continues over mainly long durations because of the sluggish rate of getting coarser. After enduring experience at higher temperatures (600–650 °C), the strength of creep in these steels reduced more rapidly than the rates calculated from short-term creep tests [5].

Zhang *et al.* [6] found that relationship between microhardness and the Prior Austenite Grain (PAG) size values and the heat treatment conditions are not able to correlate. This proposes that the Prior Austenite Grain size cannot operate an important role in temper strengthened martensitic steels. This is perceived that steel strength is mainly attributed towards precipitates, dislocations and lath structures of martensite. The important precipitates found in power plant steels are given below [7].

Table 1.2 Precipitations in creep resistant Cr-Mo steels [7].

Carbide Types	**Formula**
Graphite	C
Epsilon	$Fe_{2.4}C$
Cementite	Fe_3C
Chi	Fe_2C
Laves Phase	M_7C_3
Z-Phase	M_5C_2
M_3X	Cr_3C
M_2X	$M_2N(N,C)$ $M_{23}C_6$
MX	NbC, VC, NbN, VN

1.2.3.1 MX

It generally have the constituents of (Nb, V) (C, N) with FCC crystal structure and nucleate at martensitic grain boundaries. MX precipitates as very small particles during tempering and subsequently during creep and have a very low coarsening rate. Because of this they are highly favorable for high creep strength.

1.2.3.2 $M_{23}C_6$

These precipitates are most common and stable carbide precipitates in steels. It consists of chromium, molybdenum and iron as metal (M) and has a complex FCC structure. They nucleate during tempering of the martensitic structure along the lath boundaries and prior austenite grain boundaries which act as obstacles for coarsening by pinning the boundaries. But these precipitates have a very high coarsening rate and cease to contribute for creep strength of longer durations.

1.2.3.3 Laves Phase

These phase has a HCP structure and in the form of AB_2 $(Fe, Cr)_2(W, Mo)$. Usually precipitate at martensitic lath boundaries and prior austenite grain boundaries. It is helpful for advancing creep strength at early periods due to its soar coarsening rate they diminish W, Mo from the matrix which intensifies the strength thus weakening arise.

1.2.3.4 Z-Phase

The constituent of the this phases where Cr(V, Nb)N with tetragonal crystal arrangement. It generally precipitate as coarse particles so no contribution towards strengthening. MX phase lowers where Z-phase consumes MX phase, which will be detrimental towards creep strength. It nucleates at grain or lath boundaries or on the MX precipitates itself [3, 5].

1.2.4 Continuous Cooling Transformation (CCT)

Transformation temperature depends on chemical composition and heating and cooling rate, A_{c1} and A_{c3} temperature was found between 800-835 °C and 900-920 °C. P92 is used in the normalized and tempered condition. By cooling from austenizing (FCC) temperature to room temperature P92 undergoes complete transformation into martensite (BCT) with a maximum

hardness of less than 450Hv. This behavior is maintained over a wide range of cooling rates. M_s temperature i.e. start of martensitic transformation at around 550 °C while M_f temperature lies above 350 °C, varying as a function of initial austenite grain size [8].

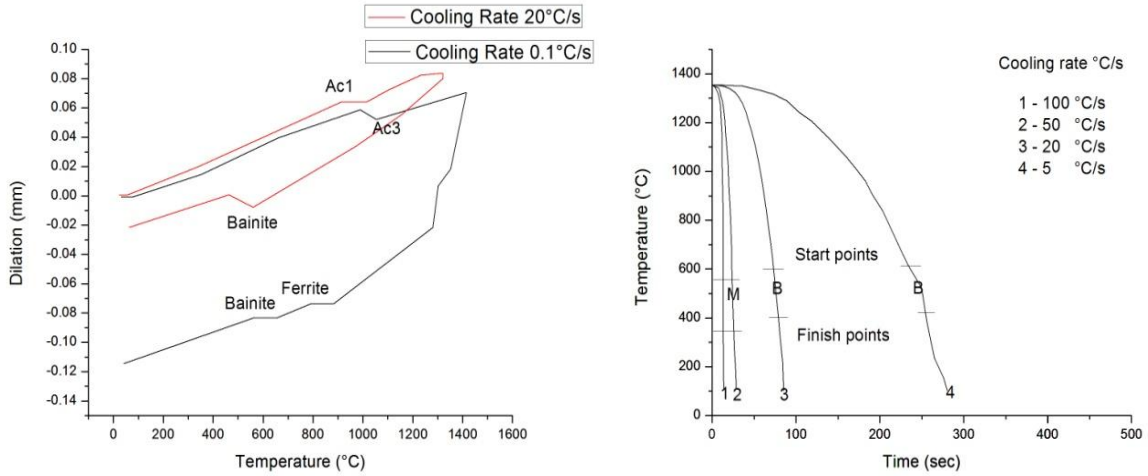

Figure 1.1 Dilation and CCT of P92 [8].

1.2.5 Advantages of P92

The advantages of P92 materials are as follows:

- P92 has lower swelling and creep rates, high strength and better thermo mechanical characters.
- Increased high temp strength and creep behavior compared to other ferritic alloys.
- Corrosion/Oxidation resistance equal to other 9%Cr ferritic steels.
- Lower aging embrittlement.
- Reduction in weight.
- Resistance to thermal fatigue.
- Good physical and mechanical properties.
- High temperature creep strength coupled with good conductivity of thermal.
- Low co-efficient of thermal expansion.
- Good stress corrosion cracking resistance in aqueous and chloride environments.

Some advantages of P92 over P91 steels

- The P92 material has 31% higher creep strength than the P91 material.
- The pipe wall thickness gets reduced for the same operating conditions. As a result there is a reduction in the material weight of around 25% at higher steam temperature ranging from 580-620 °C.
- The allowable stress for P92 is approximately 33% greater than that of P91 at 600 °C.
- With a W content of 1.8%, and V, P92 exhibits better creep rupture strength and toughness than P91 at elevated temperature conditions.
- P92 material has good anti-corrosive character and crack resistance in aqueous and gas media (hydrogen).
- Since the P92 material can operate at elevated temperatures (620 °C) the output of the power plant can be boosted up and reduces the cost of power production via usage of coal.
- Apart from distinct economical advantages which follow from the reduction in fuel consumption per unit energy generated, P92 is more eco friendly as there is a significant decrease in release of gas pollutants such as (SO_2, CO_2, nitrogen monoxide) to the open atmosphere.

1.2.6 Application of P92 Steel

1.2.6.1 Boiler Engineering

P92 is highly employed for mainstream line components such as water wall panel, headers super heater and reheater pipe works with an operating temperature of around 580-600 °C, also used for membrane water walls when boilers are burning highly corrosive coal containing complex trisulphates or vandiferrous fuels.

1.2.6.2 Nuclear Power Plants

Used in super heater sections of liquid metal fast breeder reactor (LMFBR).

1.2.6.3 Petrochemical Plants

P92 has replaced P22 plates in distillation cracking and hydro-treating units of petrochemical industries. A reason for P92 it has improved resistance to hydrogen embrittlement in thicker plates.

1.2.7 Weldability of P92

1.2.7.1 Welding and welding consumables for Cr-Mo steels

In general, creep resistant Cr-Mo steels are welded with matching consumables in order to have a homogeneous welded joint with about equal mechanical properties. Matching compositions also have the same coefficient of thermal expansion, which prevents or at least reduces the risk of thermal fatigue in service. In this respect, the heat affected zone (HAZ) is a vulnerable area.

For manual processes it is important to take sufficient measures to protect the welders from heat, and then it is of utmost importance that the preheat as well as the interpass temperatures are respected and not reduced to accommodate the welders, as well as while tacking. With the gas-shielded processes, it is vital to assure proper shielding for the weld. Over the last decades, Böhler/Thyssen Schweiβtechnik, Germany has developed a wide range of welding consumables for welding Cr-Mo steels with SMAW, GTAW, SAW, GMAW and FCAW process. A selection table for the respective welding consumables and welding processes for creep resistant Cr-Mo steels can be found in Table 1.3.

P92 has to be welded effectively with all widespread joining process GTAW, GMAW, FCAW, SAW, and SMAW covering wide range of thickness. Welding Consumables are available from several manufactures namely from Böhler/Thyssen Schweiβtechnik Thermanit MTS 616 where it’s European code EN12070 which has contented chemical and mechanical properties after adequate tempering process. Besides the strength requirements at room temperature (YS/TS) for the weld metal, it must meet defined requirements regarding toughness and strength at operating temperature (Creep Strength).

Manual metal arc is not convenient because electrode coatings tend to be hygroscopic causing weld metal porosity and there is a danger of burn through in thin gauge material.

Table 1.3 Welding consumable for Cr-Mo steels [9].

Cr-Mo Type	Base Material		Welding Consumable for Cr-Mo Steels					
	ASTM & ASME	EN	SMAW	GTAW	GMAW	SAW		FCAW
						Wire	Flux	
0.5Mo	T/P1	8MoB 5-4	Phoenix SH Schwarz 3K	Union I Mo	Union I Mo	Union S 2 Mo	UV 420 TT	Union TG Mo R
1.25Cr-0.5Mo	T/P11	10CrMo 5-5	Phoneix Chromo 1	Union I CrMo	Union I CrMo	Union S CrMo	UV 420 TT	Union TG CrMo R
1.00Cr-0.5Mo	T/P12	13CoMo 4-5	Phoneix Chromo 1	Union I CrMo	Union I CrMo	Union S 2 CrMo	UV 420 TT	Union TG CrMo R
1.25Cr-1Mo	-	15CrMoV 5-10	Phoneix SH jimper 3 K	-	-	-	-	-
-	T/P36	15NiCuNb 5(WB 36)	Phoenix SH Schwarz 3K Ni	Union I Mo	Union I Mo	Union I 3Ni Mo1	UV 420 TT(R)	-
-	-	20 MnMo-Ni 5-5	Phoenix SH Schwarz 3K Ni	Union I MoMn	Union I MoMn	Union I MoMn	UV 420 TT(R)	Union TG CrMo R
2.25Cr-1Mo	T/P22	10CrMo 9-10	Phoenix SH Chromo 2 KS	Union I CrMo 9 10 R	Union I CrMo 9 10 R	Union S CrMo 9 10 R	UV 420 TTR	Union TG CrMo 9 10 R
2.25Cr-1MoV	T/P22V	-	Phoenix SH Chromo 2 KS	-	-	Union S 1CrMo 2V	UV 430 TTR-W	-
2.25Cr-1MoVW	T/P23	7CrMoWV MoNb 9-6	Thermanit P23	Union I P23	Union I P23	Union S P23	UV 430 TTR-W	-UV P24
2.25Cr-1MoV	T/P24	7CrMo-VTiB 10-10	Thermanit P24	Union I P24	Union I P24	Union S P24	UV 430 TTR-W	-UVP24
5Cr-0.5Mo	T/P502	12CrMo 19-5	Phoenix Chromo 5	Union I CrMo 5	Union I CrMo 5	Union SI CrMo 5	Marathon 543	-
9Cr-1Mo	T/P9	X12CrMo 9-1	Thermanit Chromo 9V	Thermanit MTS 3	Thermanit MTS 3	Thermanit MTS 3	Marathon 543	Thermanit MTS 3 PW
9Cr-1Mo mod.	T/P91	X10CrMoV Nb 9-1	Thermanit Chromo 9 V Thermanit Chromo T91	Thermanit MTS 3	Thermanit MTS 3	Thermanit MTS 3	Marathon 543	Thermanit MTS 3 PW
9Cr-0.5MoWV	T/P911	X11 CrMoWVNb 9-1-1	Thermanit MTS 911	Thermanit MTS 911	Thermanit MTS 911	Thermanit MTS 911	Marathon 543	-
9Cr-0.5MoWV	T/P92	X10CrWMoNb 9-2	Thermanit MTS 616	Thermanit MTS 616	Thermanit MTS 616	Thermanit MTS 616	Marathon 543	-
12Cr-0.25Mo-1.4W13Co0.2V	-	X12Cr CoWVNb 11-2-2 (VM12-5HC) t<10mm	Thermanit MTS 5 CoT	Thermanit MTS 5CoT	-	-	-	-
12Cr-1Mo-NiV	-	X10Cr-MoV11-1	Thermanit MTS 4	Thermanit MTS 4 Si	Thermanit MTS 4 Si	Thermanit MTS 4	Marathon 543	-

With this process and with gas welding, there's always the risk of flux entrapment in the joints which can reduce the corrosion resistance. Gas welding is a slow process and can give uncontrollable distortion. The more concentrated heat input of the GTAW process as compared to gas welding enables welding speed to be increased, distortion can be minimized and the metallurgical quality of the weld like toughness can be improved. Pure tungsten electrodes are less expensive, low current carrying capacity, low resistance to contamination. They are generally used on less critical application, compared to pure tungsten electrodes, thoriated ones have higher emissivity, better conductor of electricity, durability, greater contamination resistance, with this electrode arc striking is easier and arc is more stable. Zirconiated electrodes have properties intermediate between the above two and its being used to weld P92 while welding with AC they are found to work better than the others [9].

To correlate its mechanical properties and chemical composition of weld metal every single element had been studied by researchers and optimized nitrogen, nickel, manganese, columbium, and boron. By forming carbonitirdes in the weldment, it has been found nitrogen has important influence in creep strength as also for boron with increment in yield and ultimate tensile strength but lessens ductility and toughness. Excess Ni and Mn content improve the ductility considerably but they can influence on A_{C1} temperature they have to be limited with a sum of 1.5%. Cobalt can be used as substitute for Nickel because of the α/γ transformation points [10].

Zhang *et al.* [6] had cited that in the TIG welding of the T91 observed that the fusion Zone (FZ) has duplex structure of martensite laths and ferrite grains, which could be due to faster cooling rate after welding. Tungsten has to be minimized in the filler metal to reduce the delta (δ) ferrite in the weldment which is detrimental to boiler application. Similarly vanadium and niobium have undesired effect on hot cracking in the weldment so their percentage has to be shrunk. In addition to this aluminium, titanium is also added due to their formation of nitride compounds in the weldment.

Onoro [11] had reported that to get fully martensitic weld metal microstructure in 9-12%Cr, it requested to lessen the ferrite forming elements. The partial substitution of Mo for W lessens the delta ferrite appearance that accelerates the mechanical behaviour at high temperatures. Co is recommended as an austenetizing element. Ferrite formation can be reduced by Co, thus leads to increase the strength of creep and toughness where M_s temperature will not be affected.

1.2.8 Heat treatments for Cr-Mo steels and welded joints

The heat treatments for the base materials are reasonably complex but are required to obtain the optimal mechanical properties. Depending on the alloy content a normalising, tempering and annealing treatment at various temperatures for several hours with a controlled cooling rate have to be executed according to ASME section 1. The same is valid for the weldmetal, with increasing alloy content the Post Weld Heat Treatment (PWHT) for welded joints gets more complicated as illustrated in figure 1.2. When in subsequent PWHT, Intermediate Stress Relieving (ISR) or in service, the ultimate heat treatment temperature of the base material is exceeded too much and too long, the precipitations can dissolve again which causes reduction of the mechanical properties of the base material. This implies that, for this reason the maximum temperature of 760 °C for P92 in figure 1.2 shall not be exceeded.

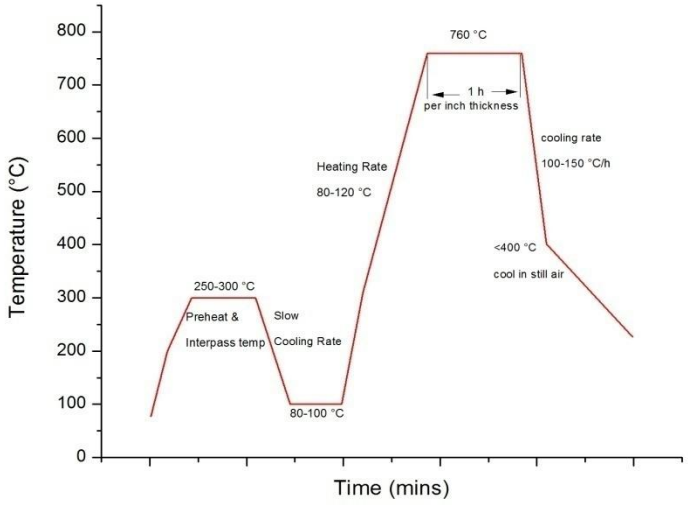

Figure 1.2 Heating cycle for weld [3].

Depending on the alloy level, from only 0.5%Cr to 12%Cr-1%Mo the welding condition regarding preheat and interpass temperature as well as the subsequent temperature cycles during Stress Relieving (SR), ISR, Step Cooling (STC) and PWHT´s change drastically. It has been recommended in ASME pressure and boiler vessels that PWHT should be atleast 100 °C above than the operating temperature [3].

1.2.9 Heat Affected Zone (HAZ) Subzones

In order to understand the types of cracking in and around steel weldments it is necessary to understand HAZ subzones that are formed when creep resistant steels are welded that are briefed in the following table 1.4 and figure 1.3.

Table 1.4 HAZ subzones and its characteristics [4].

Sub-Zone	Peak Temperature (°C)	Remarks
Coarse Grained HAZ (CGHAZ)	>1250	Precipitate dissolves completely, thus having no pinning effect on austenite grain growth. It transforms back to austenite upon cooling. However, the cooling rates are very high which might lead to presence of delta ferrite. It has the highest hardness of HAZ and is vulnerable for reheat cracking.
Fine Grained HAZ (FGHAZ)	~1100	Because of low peak temperature, dissolution of precipitates is incomplete. Thus, concentration of carbon in the solution does not increase because of which hardness & strength doesn't increase significantly which makes it the weakest zone after cooling to room temp.
Inter-critical HAZ (ICHAZ)	Between A_{c1} (800) and A_{c3}(950)	There is a transformed martensite which is fine grained and an untransformed martensite which is overtempered present in this region.
Over Tempered (OT)	Just below A_{c1}	Precipitates coarsen accompanied with recovery and annihilation of dislocation. There is no phase transformation here.

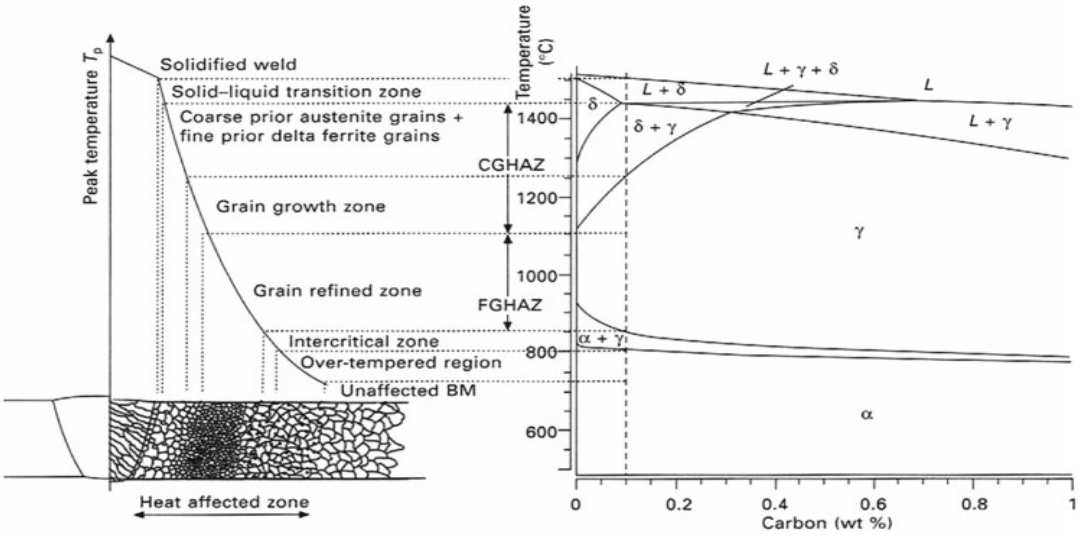

Figure 1.3 Subzones of HAZ after welding [4].

1.2.10 Crack types in steel weldments

High temperature steel gained its strength from solid solution strengthening, dislocations, substructure strengthening and precipitation strengthening.

1.2.10.1 Type-I&II crack

They occur rare in P92 steel welds where most prevalent in nickel base alloys and austenitic stainless steel.

1.2.10.2 Type-III crack (reheat crack)

Most common in austenitic stainless steel, not common in high alloy steels like 9-12Cr%. Inter-granular reheat cracking occurs due to segregation of elements along the prior austenite grain boundaries thus lowering the cohesive strength. In welding all precipitates get dissolve in CGHAZ and again they develop during PWHT or at high temp creep. The coherent precipitates like MX will precipitate inside the grain and hinder the dislocation motion where as non-coherent precipitates like $M_{23}C_{6,}$ Fe_3C, M_6C will get precipitate on the grain boundaries and gives pinning effect.

Sooner these precipitates coarsen due to high diffusive grain boundaries (GB) and the solid solution strengthening along GB become weak which result in creep crack fracture during high

temp loading and also due to residual stress relief during operation or PWHT. The recovery of dislocations during PWHT will also induce localized stress concentration around them and make the boundaries vulnerable to failure. Since, then it has many conflicts towards failure for discussion.

1.2.10.3 Type-IV crack

Heat affected zone (HAZ) exhibits Type-IV crack that results in the limitation of components life. Brief insight was carried out to know the cracking phenomena so as to ease this problem. Creep tests executed on the welded steel exposed the type IV crack in the fine grain and inter-critical heat affected zones. These confine creates localized deformation that leads to the prominent creep cavitations in the ICHAZ of the weld joint to yield type IV failure. The creep life lessening due to type IV cracking in the HAZ depends on the applied stress and test temperature. Weldment creep cracks have been classified on the basis of their points of origin as shown in the figure 1.4 [4].

At lower stress levels creep fracture location is shifted in to very narrow FGHAZ or ICHAZ region called Type-IV cracking. It's the major problem for end of life for high temperature materials which is why researchers are investigating its phenomenon. This type of cracks are stated in low alloy ferritic/martensitic or bainitic steels like as 9-12%Cr like P91, P92, P122 and E911. The time of rupture for failure by Type-IV cracking is susceptible to the stress state and the applied loading direction. The failure mechanism of Type-IV is governed by creep cavitations. Parker *et al.* [12] had measured the grain dimension in the failed part and concluded that localized strain of 20-30% was present in the FGHAZ region when the overall strain is only 10% with ductile failure in nature. Creep voids commenced at sub-surface preferably along prior austenite grain boundaries where it has fine grain boundaries instead of lath martensitic structure. These voids diffuse perpendicular to the applied forces and coalesce to form micro cracks and then to macro cracks. Nucleation site can be interface of particle and matrix associated with inclusion of second phase particles. Due to weld thermal cycle new precipitates occurs on partially dissolved precipitates such as $M_{23}C_6$ instead of re-precipitation at grain boundaries to reduce the interfacial energy. These preserved particles grown to coarser more fast in IC/FGHAZ during PWHT and become nucleation site for creep voids which reduces the creep rupture strength by grain boundary weakening.

Some significant factors which have been identified for the cause of Type-IV cracking are

1. Partial dissolution and coarsening of precipitates.
2. Equiaxed grains instead of lath martensitic structure.
3. Intermetallic Laves Phases Fe_2(W, Mo) precipitated along GB during the activity of creep which becomes nucleating site for creep voids. W and Mo contents got exhausted due to laves phase coarsen effect.
4. Z-phase formation by dissolution of intra-granular elements like (V, Nb) + (C, N) in the ICHAZ due to longer high temp creep exposure.
5. Dynamic recovery of dislocations which increases strain locally and soften the region.
6. Finer prior austenite grains - This shows more GB per unit area so energetically more rapidly recovery can happen. Faster recovery can happen at GB than Sub grain boundaries because of higher internal stress and energetic.
7. MX carides or carbonitrides coarsen by ostwald ripening mechanism where the creep get accelerated [13, 14].

As in-depth understanding of Type -IV creep crack is critical for successful induction of P92 alloy in power plants. In the current work the susceptibility of Type-IV crack in the FGHAZ and ICHAZ will be investigated by using the simulation process with Gleeble® 3800 thermo-mechanical analyzer.

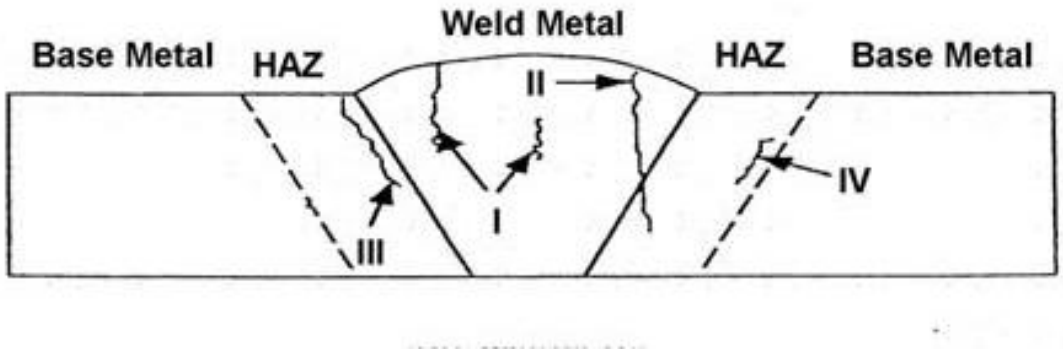

Figure 1.4 Crack types in weld joints [4].

Table 1.5 Classification of cracks in steel welds [8].

Crack Type	Origination	Propagation
Type-I & II	Weld Metal	Type I will propagate in weld metal and Type II will propel towards HAZ or base metal too.
Type-III	Coarse grained HAZ very close to WM	May spread in to base metal
Type-IV	FGHAZ/ICHAZ	May spread within the section to cause early breakdown. Most common in Cr-Mo steels.

Vaillant *et al.* [1] had reported that low C percentage provides better weldability, which sometime avoids PWHT for slim products like tubes for water wall panels or superheaters. V, Nb addition (or V, Ti for grade 24) combined with C/N to form carbides, nitrides and/or carbo-nitrides of MX type and creates a fine precipitation in the matrix that increases the materials strength. Tungsten is added (at reduced Mo content) to further improve the creep resistance.

Ram *et al.* [4] stated that Mo is twice that of W for ferrite stabilizing and are important constituent for laves phase. An increase in any of the element will rapidly increase the fraction of laves phase but Z phase remains unaffected hence partial replacement of Mo with W is expected to increase the creep strength up to some extent but limited tungsten will create local delta ferrite in P92. Cr increases the amount of laves phases and also Z-phase.

Laha *et al.* [13] have reported coarsening of $M_{23}C_6$ and Z-phase precipitate at the expense of MX carbides at soft inter-critical HAZ results in the premature creep failure in grade P91. Test result showed that 10%, 18%, 30%, 45% reduction in creep strength at the corresponding temperatures as follows 525, 560, 600, 650 °C compared to base metal strength. TEM image showed in figure 1.5, that weld thermal cycles changed lath martensite with high dense dislocation into subgrains with low dense dislocation. ICHAZ has the lowest hardness in the weld joint of the steel.

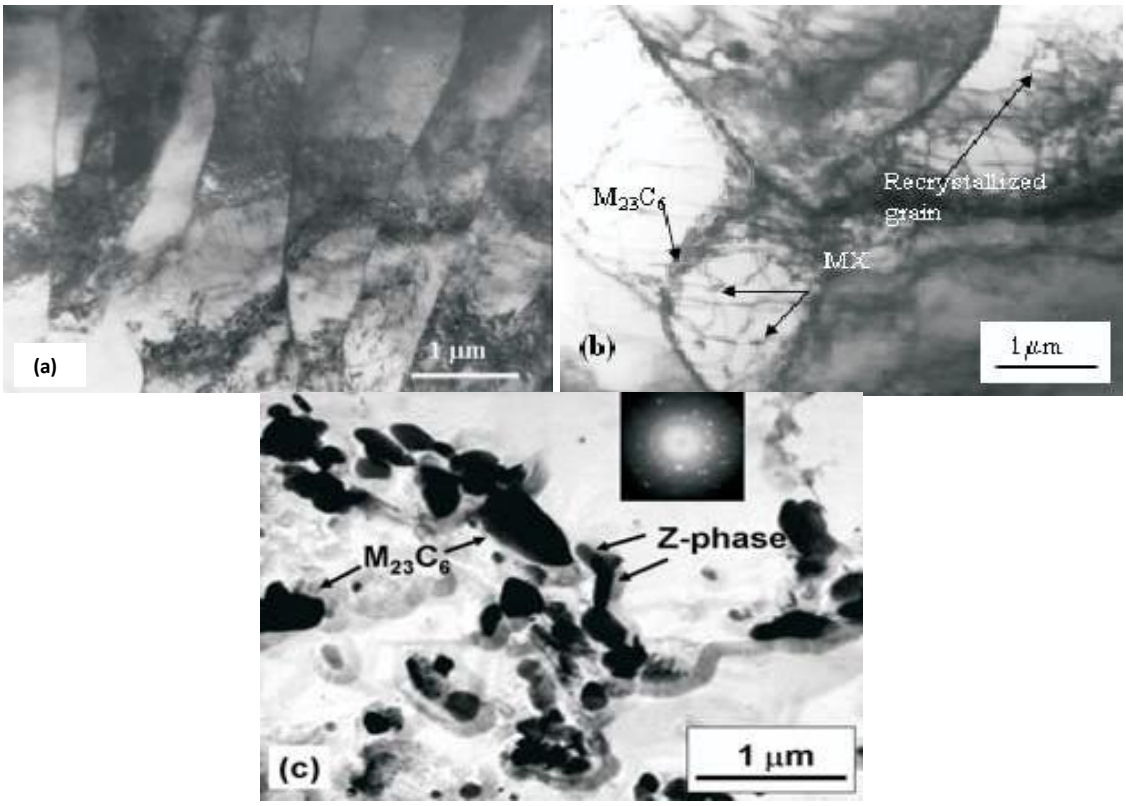

Figure 1.5 (a) Lath martensitic structure in modified 9Cr-1Mo base metal (b) Recovered subgrain structure in inter-critical HAZ and (c) Z-Phase in the inter-critical HAZ [13].

Recent growth lead to create novel steel grades like T/P911 (European E911; X11CrMoWVNb9-1-1) and T/P92 that had enhanced mechanical properties at elevated temperatures, especially, a raise in strength of creep to 10–30% in 100,000 h at 600 °C and thermal fatigue which is why it can reduce the wall thickness of the pipes to get economical compensation on tubes and pipes pricing.

Kim *et al.* [15] had explained as the crack growth path of HAZ grew along the CGHAZ adjacent to fusion line and many voids were noticed around the crack tip causes stress relaxation and acceleration of creep growth. The creep rupture life and the crack growth rate of HAZ were shorter and faster than those of base metal. Also, the creep rupture position of HAZ specimen is the ICHAZ region by the interrupted creep rupture test, and many cavities observed at the ICHAZ.

Fournier *et al.* [16] observed cyclic softening and decrease in dislocation during creep fatigue test by controlled strain cyclic test in base metal (BM) P92, creep occurs by necking at high temperature of 600 °C for 100000 h. TEM results showed that fade of low angle boundaries and decrease in dislocation densities by visco-plastic deformation due to dislocation climb or glide and also new precipitates formed as Cr_2X with N and W. In as-received condition, BM has a precipitate of $M_{23}C_6$ of 100 nm at high angle boundaries which pin GBs, MX precipitate that are V/Nb rich at matrix and GB of 15-20 nm and also carbo-nitrides. Sub-grain diameter has been calculated with TEM as received 0.43 micron and after creep fatigue 0.7micron and dislocation densities for both as 2×10^{14} m^{-2} and 1×10^{14} m^{-2} at 550 °C, where sub-grain grows by 1.8 times for P92. Cyclic softening was observed in all ferritic-martensitic steels during comparison of creep fatigue test where P92 has some better extent.

Mandziej [17] developed a creep test using thermo-mechanical fatigue using Gleeble® physical simulator, the compositions of precipitated phases contains mainly carbides, could reach in less than 30 hours the state near to the thermodynamic equilibrium, as predicted by Thermocalc. The loss of strength in the martensitic-ferritic steels is associated with transformation of microstructure due to precipitation and coagulation of carbides and formation of intermetallic phases as well as recovery and recrystallization of matrix. The developed accelerated creep test obeyed the following principles:

1. The basic temperature and applied strains prevent odd transformations like secondary dissolution of carbides or intensive formation of non-equilibrium phases.
2. The final deformation at fracture is like at real creep – just a few % in total.
3. The depletion of weld metal or steel matrix in alloying elements is achieved similar to that of crept steels and the carbide phases at onset of cracks are not different.

1.2.11 Sysweld

Finite element method (FEM) of recreation is the best way to approach a master design, manufacturing process and in-service problems at the earliest product stage possible. SYSWELD-2003 is the leading tool for computer modeling of physical effects that are related to heat treatment and welding. Software allow us to simulate different ways of welding with input of all material properties depending on temperature, phase transformation, proportion of

chemical elements, design, process and auxiliary variables. Typical applications include by hand MIG/MAG, TIG, by laser, resistance spot welding, etc. With sysweld, it's possible to simulate laser heat treatment, electric beam, induction heat treatment, standard welding, yielding and thermochemical heat treatment like nitriding or carbo-nitriding, etc. Software Sysweld is simple and user friendly. A dynamic volumetric heat source has been considered for modeling of welding arc, based on the double ellipsoidal proportion proposed by Goldak *et al.* [18] proposed a heat source model as in figure 1.6 was used, where x, y and z are the local coordinates of the double ellipsoid model aligned with the weld line. During modelling the fraction of heat deposited on the rear and front of the welding arc should be measured, it should be observed that much steeper temperature gradient at the front of the arc than that of the rare. Losses of Heat due to thermal radiation and heat transfer on the weld surface have been considered. Losses by radiation are more at elevated temperatures near and in the weld zone, and loss by convection for lower temperatures away from the weld zone.

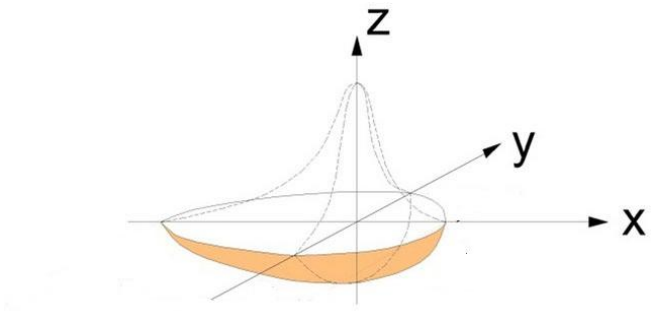

Figure 1.6 Double ellipsoidal heat source [19].

The results of the welding simulation by sysweld are as follows [19]

1. Temperature field and gradient.
2. Phase proportions.
3. Hardness.
4. Distortions.
5. Residual Stresses.
6. Plastic Strain.
7. Yield stress depending on the mixture of metallurgical phases.

1.2.12 Physical / thermo-mechanical simulation

Physical simulation is a method of attempt to replicate the real world process on a laboratory scale in a way that the resultant data can be used to solve real world problems. All the physically simulated samples can be used for physical testing. Thermo mechanical simulation can indeed be a useful development tool in the hands of those fully aware of its capabilities and limitations, and the Gleeble® is the most well-known physical simulator. In the absence of standards, mistakes in simulation can be made and incorrect conclusions can be drawn.

Weldability tests from the welding institute (TWI) have been designed with the same straight HAZ idea. However, the thermo-mechanical simulator can create a homogenous single microstructure within a large volume of material, thus testing separately the properties of the coarse-grained HAZ, inter-critically reheated HAZ, etc. The temperature measurement system measures the instant temperature of the specimen through a thermocouple.

Additionally real time experiments introduce many sources of error due to differences in operator expertise, heat transfer efficiency changes from one process to another, and many other operator-related variables. On the other hand, the Gleeble® is based on a computer controller that reliably sends and adjusts control signals and acquires up to 2000 samples per second. Under normal circumstances, it operates with great accuracy and reproducibility. When introducing cooling rates in these models, predicting of microstructures is also possible [20].

Heat Affected zone simulation can be performed by in-built heat transfer equations such as Hannerz Equation, Rykalin 2D and 3D equations, Rosenthal Equations. Xue *et al.* [21] had reported that FGHAZ microstructures had been replicated by heat treatments in a furnace and by using a weld simulator. Simulated fine grained heat-affected zone (FGHAZ) specimens at temperature of 930 °C for P92 welded joints were compared with heat treated, there were difference in microstructure and creep properties of the simulated FGHAZ obtained by this two simulation methods for P92 steel then the creep tests were passed out at 650 °C under the applied stress of 90-120MPa to examine elevated temperature creep FGHAZ behavior.

Experimentally for P92 HAZ simulation the properties and microstructure of the simulated samples didn't correlated with real time. So in this work we have idealized to create a weld thermal cycle simulation by using finite element modeling and with the obtained thermal cycle's program can be generated for the Gleeble® input with software called Quicksim® associated with Gleeble®.

Chapter - 2

Experimental Procedures

Investigation on different series of heat input for sound weld of P92 with electrode Thermanit MTS616 from Böhler/ThyssenSchweiβtechnik, Germany using GTAW process from Kemppi machines was determined. Heat Affected Zone (HAZ) of weldment that varies with microstructure which depend on the thermal gradient and peak temperature experienced at that particular location where simulated using sysweld software for thermal cycle simulation of peak temperature, this peak temperature physically simulated using Gleeble® thermo-mechanical Simulator. To understand and compare the real and simulated peak thermal cycles, macrostructure, microstructure, micro-hardness, toughness test, tensile test, bend test on weld were characterised.

2.1 GTAW Welding of P92

GTAW welding has been chosen due to its concentrated heat input, less spatter, faster than other methods so it results in less heat affected zone area though it has less efficiency of 50% than other process [22]. Zirconated tungsten electrode has been used because of its good emissivity and less contamination with good current carrying capacity and Cold Wire TIG with DCEN-straight polarity which gives good penetration for the weldmetal pool where more heat is absorbed by external filler metal and less heat to the base metal. Oscillation of 3.5 mm during welding of 2^{nd} and 3^{rd} passes was given to reduce the number of passes. Argon has been used as shielding gas to protect the weldmetal from external atmosphere for weld defects with a flow rate of 8-20 litres per minute (LPM).Purging of argon was inside the pipe to protect the weld pool from oxidization and also improves corrosion resistance with a flow rate of 3-12LitersPerMinute (LPM). Weld trail has been performed with various parameters like current, travelling speed (S), Wire feed rate (WFR) and no of passes. Electrode from Böhler/ThyssenSchweiβtechnik Thermanit MTS 616 of diameter (Ø) 0.8 mm where its European code EN12070 has been used [23].

2.1.1 Edge Preparation

For higher thickness materials, joint convenience must be provided for welding to ensure weld soundness and strength while welding with GTAW, so edge has been prepared for the pipe material which has thickness of 5 mm and internal diameter of 35 mm and external

diameter of 45 mm with V-groove angle of 75° according to AWS/ASME standards as shown in figure 2.1 below.

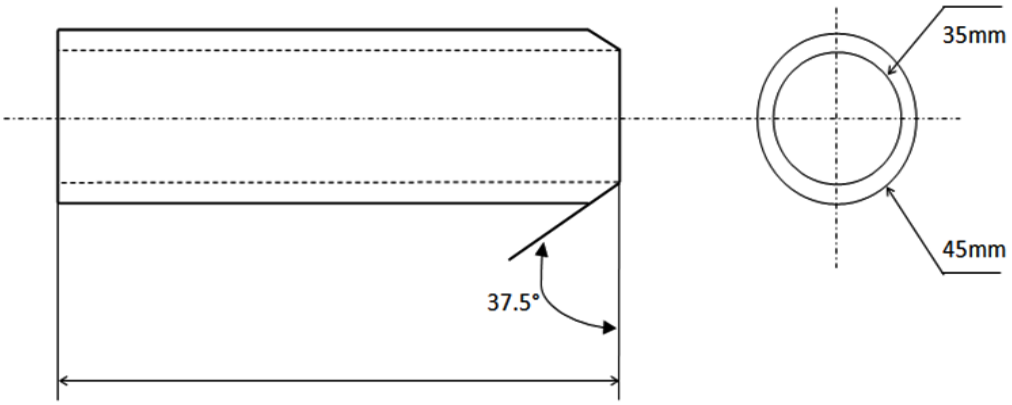

Figure 2.1 Edge preparation.

2.1.2 Preheat

Application of preheat, to increase the temperature of the parent steel before welding to reduce the risk of cracking induced by diffusible and residual hydrogen in the weldment mainly to reduce the weld and base metal cooling rate, resultant softer weld metal and heat affected zone microstructures had shown a greater resistance to hydrogen cracking during fabrication. The sluggish rate of cooling results in effusing hydrogen out of the weldment and High temperature long duration of HAZ area at temperature above 100 °C is feasible for higher hydrogen diffusion rates thus hydrogen reduction reduces the cracking risk.

Preheat can be applied by various process which depends on material thickness, weldment size. Preheat has been applied to 5 mm thick pipe material by oxyacetylene gas heating with neutral flame to a temperature of 150-250 °C.

2.1.3 Post-Weld Heat Treatment (PWHT)

Post-weld Heat treatment means heating and soaking after welding at some required elevated temperature to get better, the properties of a weldment. In concept, PWHT can include many diverse possible treatments; though, for fabrication of steel, procedures frequently used were stress relieving and post heating. The PWHT need is standardised by code and application needs, as well as in-service environment. In general, when PWHT is necessary, the purpose is to enhance the resistance to brittle fracture by relaxing residual stresses. Hardness reduction and material strength enhancements are also desired results from PWHT. Post heating is to

minimize the hydrogen induced cracking (HIC) potential. After complete welding, the steel should not be cooled below 80-100 °C before it should be heated from the interpass temperature to the post heat temperature of 760 °C and held at this temperature for 30mins minimum in accordance with AWS D10.10M and ASME boiler and pressure vessel code Section 1[24].

2.2 Welding Parameters (Trial)

Table 2.1 Welding trail:

Current (I)	Voltage (V)	No. of Passes	Travel Speed (S) (mm/sec)	WFR (mm/min)	Heat Input (J/mm)
140/130-2 passes	12.5	3	2.21	800	807/750
135/135-2 passes	11.5	3	2.21/2.10	800	716/741
125/115-2 passes	12.5	3	2.09	800	747/687
110/100	12.5	2	1.47/1.51	2220	819/841
120/110	11.5	2	1.68/2.01	1200	738/597
100/100	11.5	2	1.12/1.31	2000	798/871
115/100	10.5/12.5	2	1.14/1.39	1400	821/893
115/100	10.5/12.3	2	1.22/1.41	800	898/721

2.2.1 Optimised Weld Parameters

Table 2.2 Optimised parameters:

Variables	Numericals
Current (RP/FP)	110/100 Amp
Voltage	9-12.5 V
Polarity	DCEN
Wire Feed Rate (WFR)	2220 mm/min
Gas Flow Rate (Shielding/Purging)	16/6 LPM
Travelling Speed	1.47/1.51 mm/sec.
Preheat/Interpass Temperature °C	200 °C
Heat Input $1^{st}/2^{nd}$ pass	819/841 J/mm

2.3 Sample preparation for weld evaluation

After welding, nondestructive examination (NDE) of samples using radiographic testing was carried out for finding presence of any discontinuities during welding. After NDE, the samples were cut into exactly two halves exactly perpendicular to the weldment and one half for heat treatment.

2.3.1 Optical microscopy for macro and microstructures

Abrasive cutting of metallographic specimens was performed using a water-cooled abrasive cutter (Metco, Chennai) and samples for optical microscope examination were cold mounted. Following mounting, samples were subjected to manual grinding using 80, 120, 150, 220, 320, 400, 600 and 800 grit silicon carbide papers in succession. When the grinding step using 800-grit was completed, the sample was cleaned in acetone and dried with hot air.

The ground samples were further polished using alumina polishing. After the final polishing, the samples were ultrasonically cleaned in acetone and dried with hot air again. The polished samples were etched using either viellal's or Waterless Kalling's reagent with different

etching time used for macroscopic and microscopic analysis according to the standard ASTM E407.

2.3.2 Mechanical Testing of Weld

2.3.2.1 Micro-Hardness Test

Vickers's hardness measurements were taken using AFFRI (model WIKI 200JS) with a load of 300grams and 10 second dwell time. The hardness survey begins in the weldmetal, and ran through the HAZ to the unaffected base metal, to illustrate the hardness variation in different regions by simulating the same welding parameters without the application of load. ASTM E384-05 guidelines were followed for measuring hardness.

2.3.2.2 Tensile Test

An axial hydraulic and computer-controlled Universal Testing Machine (UTE 60, Make Fuel Instruments and Engineers (FIE), India) unit with a capacity of 60,000 kgf was used to estimate tensile properties like yield strength (YS), ultimate tensile strength (UTS), and ductility parameters such as percentage elongation (%El) and percentage reduction in area (%RA) at room temperature along with atmospheric conditions according to the AWS B4.0 and ASTM designation E8 Transverse weld tensile test specimen.

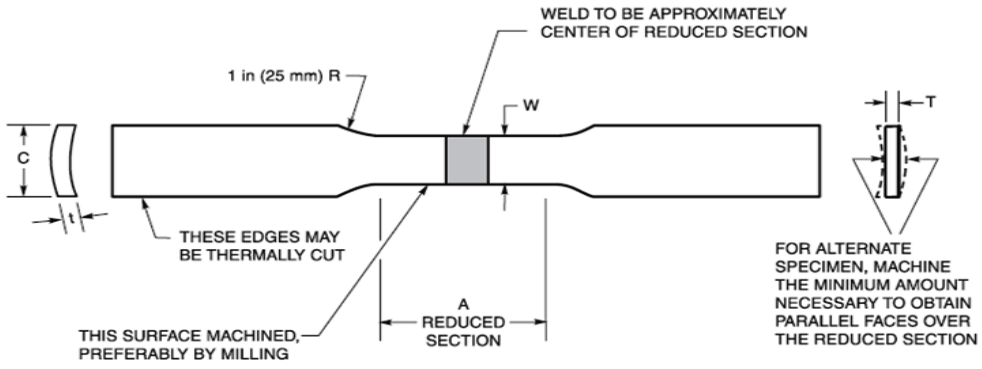

Specimen No.	W in (mm)	C in (mm)	A in (mm)
1	1/2 ± 1/64 (13 ± 0.4)	3/4 (19) approx.	2-1/4 (60) min.
2	3/4 ± 1/32 (20 ± 2.4)	1 (25) approx.	2-1/4 (60) min. 4-1/2 (115) min.
3	1 ± 1/16 (25 ± 1.6)	1-1/2 (38) approx.	2-1/4 (60) min. 4-1/2 (115) min.
4	1-1/2 ± 1/8 (38 ± 3.2)	2 (50) approx.	2-1/4 (60) min. 4-1/2 (115) min. 9 (229) min.

Figure 2.2 Reduced rectangular section tension specimens for pipe.

2.3.2.3 Bend Test

A uniaxial hydraulic controlled universal testing machine unit was used to determine ductility and defects in bend side. The specimens are guided in the bending process by a test fixture that employs a mandrel with wraparound roller or end supports with a plunger. The ductility of the welded joint, as evidenced by its ability to resist tearing and the presence of defects on the tension surface at ambient temperature and atmospheric conditions, is determined in a guided bend test in accordance with the standard ASTM E190. The radius of the mandrel has determined by the following equation

$$A = T(50/e - 1/2)$$

where
A = Radius of mandrel or plunger, ±1.6 mm);
e = Elongation at outer surface, % ±1%; and
T = Specimen thickness, (±0.40 mm).

2.3.2.4 Impact Test

Charpy V-Notch impact test of welded samples has been carried out in subsize samples ((55×10×5) all dimensions are in mm) as shown in figure 2.3 with notch angle of 45° and depth of 0.25 mm (±0.002 mm) to determine the toughness of the welded joint at ambient temperature and atmospheric conditions. Results has been reported according to the standards ASTM designation E23 and AWS B4.0

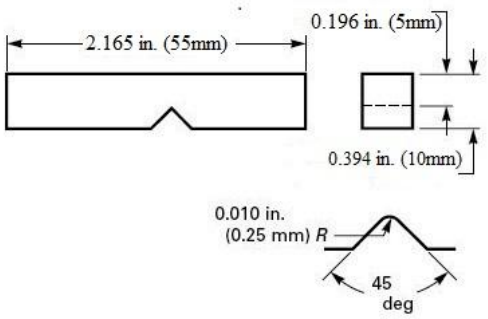

Figure 2.3 Charpy test subsize specimen.

2.4 Sysweld-FEM

Weld thermal cycle simulation is a Finite Element Method which is derived by fitting double ellipsoid heat source fitting tool as shown in figure 1.6 along with weld parameters, material physical and mechanical properties it simulates region of thermal field and gradient, phase

proportions, hardness, distortions, residual stress, plastic strains, yield stress depending on the mixture of metallurgical phases, peak temperature at a particular point.

The Poisson's ratio, Young's modulus, Yield strength, thermal expansion, thermal conductivity, specific heat and density at various temperatures were extrapolated and measured for the simulation of welding process with Thermal Properties Analyzer according to the ASTM standards ASTM E1876, ASTM E228, ASTM E1225, ASTM E132, respectively [25]. Poisons ration was taken as 0.28.

Table 2.4 Temperature dependent physical properties of P92.

Temperature (°C)	Thermal Conductivity (10^{-1}J/s/mm/°C)	Density (10^{-2} g/mm)	Specific Heat (J/g/°C)
20	0.276	0.786	0.423
100	0.283	0.781	0.430
200	0.286	0.781	0.462
300	0.290	0.776	0.483
400	0.293	0.774	0.513
500	0.297	0.774	0.586
600	0.3	0.760	0.604
700	0.323	0.762	0.637
800	0.344	0.751	0.653
900	0.281	0.725	0.683
1000	0.274	0.713	0.702
1200	0.281	0.704	0.723
1300	0.286	0.7	0.730
1400	0.295	0.674	0.739
1500	-	0.616	0.741

Table 2.4 Temperature dependent mechanical properties of P92.

Temperature (°C)	Thermal Expansion Coefficient (10^{-7}/°C)	Elastic Modulus (GPa)	Yeild Strength (MPa)
20	158.283	212.331	454.306
100	162.416	196.221	423.379
200	168.254	191.208	413.424
300	173.840	178.779	399.769
400	177.251	162.655	381.173
500	180.514	147.762	331.718
600	182.125	139.042	248.922
700	181.711	117.977	182.212
800	182.371	106.788	122.915
900	187.791	94.2904	103.082
1000	199.680	45.9898	39.9694
1200	205.206	16.2019	29.9404
1300	212.336	212.331	13.3142
1400	219.388	196.221	5.09073

2.5 Physical Simulation-Thermo Mechanical Simulator

The thermo-mechanical Simulator or physical simulator – Gleeble® 3800 shown below facilitates superior physical thermo-mechanical experiments, such as material testing at high temperature tension/compression, dilation, phase transformation, Strain induced crack opening (SICO), process simulation like Heat Affected Zone by weld thermal cycles, heat treating, continuous casting, hot rolling among other. It permit us to execute straightforward or intricate thermo-mechanical treatment on conducting materials while access the material thermal, electrical and mechanical response, at the same time that phase conversion can be tracked with dilatometer. This results in establishing continuous cooling transformation

(CCT) diagrams for materials, to simulate materials processing conditions, as cold/hot rolling, forging, melting, welding (single and multipass heat affected zone simulation [26].

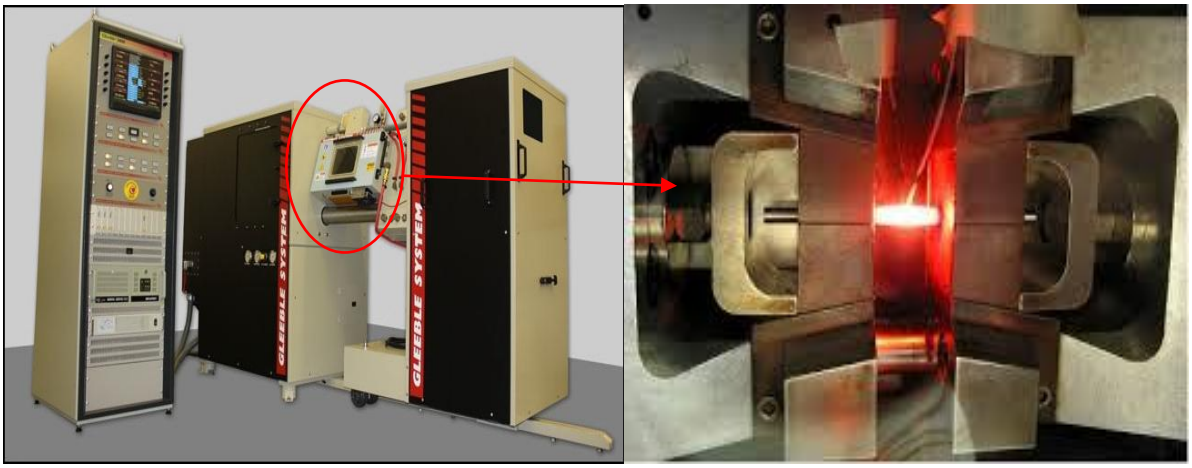

Figure 2.4 Gleeble® 3800 thermo mechanical simulator and simulating sample.

The physical simulator equipped with a hydraulic system of load capacity 20 tons in compression and 10 tons in tension. Heating is done by the Joule effect i.e. the heating that occurs when an electric current flows through a resistance, which provides heating rates of up to 10,000 °C/s. For cooling, the machine comes with copper jaws favouring the accelerated cooling and accessories enabling to use water, air, inert gas or liquid nitrogen to even higher rates and for tension and compression it has AISI 304 hot jaw, Half contact jaw, Full contact jaw. For testing requiring precision in displacement and dilatation, it is possible to use accessories such as extensometers and dilatometers.

The temperature measurements done by two methods: thermocouple (K, S, R, B types, etc.) or pyrometer. Pyrometers are two types as single colour and two colour, but not preferred because single colour has lower minimum temperature range, while two colour is typically not as sensitive to emissivity change where as thermocouple has faster thermal response time than pyrometers, so when high heating rate is required, thermocouple is usually used where the thermocouple works on patented time sharing technique i.e. temperature measured when current is not flowing through the specimen. Gleeble® system has Ø-0.2 mm thermocouple. Thicker wire will reduce the response time and accuracy. Thermocouple should be welded in middle of the specimen 1 mm apart in the same cross section perpendicular to specimen axis to form a good junction otherwise; different voltage potential along the specimen axis will lead to temperature measurement error. To measure the specimen temperature correctly

thermocouple has to have an intimate contact with the specimen so during thermocouple welding following measures has to be taken

1. The specimen surface must be clean with no grease, no scale or machine oil
2. The specimen must be in good electrical contact with the specimen holder in the welder
3. The thermocouple wire must be in good electrical contact with the drop arm of the welder

2.5.1 Effect of Free Span

The temperature distributions along the specimen using copper jaw at a different free span of 10 mm to 40 mm were investigated by Dynamic System Inc.,

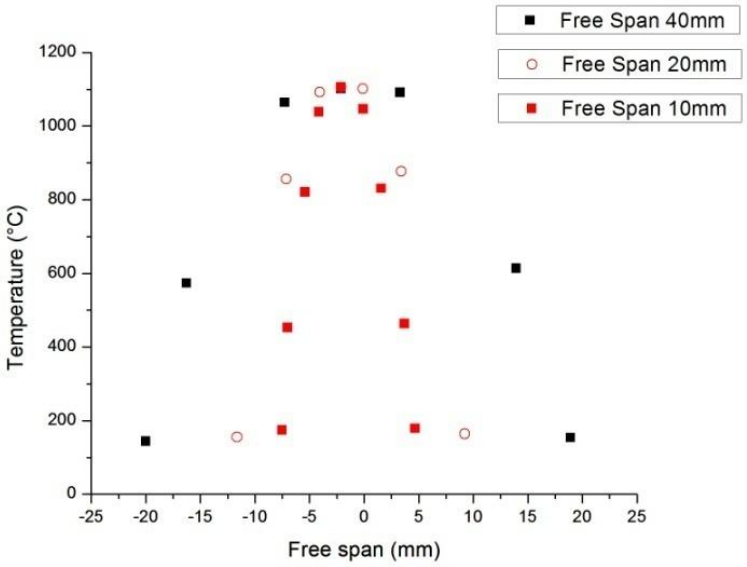

Figure 2.5 Temperature distributions along the specimen at different free span [26].

It is evident that a short free span exhibits steep temperature profile over the free span but if we increase the free span the desired cooling rate cannot be achieved by water or air cooled via copper jaw for HAZ simulation, so it is advised to have a free span of 10 mm for HAZ simulation processing. As the free span becomes shorter, thermal gradient increases rapidly. A thermal gradient of 200 °C/mm has been obtained at a free span of 10 mm using water cooled copper jaw, which is sufficient for welding HAZ simulation.

2.5.2 Grips

Copper grips are normally used for HAZ simulation because of its greater thermal conductivity, when loading a specimen the thermocouple must be located in the middle of the free span, and the grips must be clean, otherwise the thermal profile of the specimen will not be symmetrical.

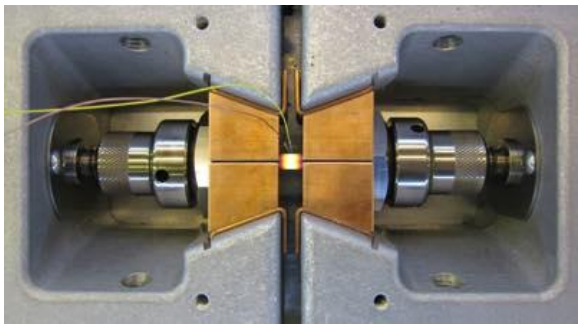

Figure 2.6 Water-cooled copper grip contribute to very fast cooling rates and enable to simulate steep thermal gradients found in welding applications.

2.5.3 HAZ Simulation

HAZ simulation can be performed by using table programs which integrated with Quicksim program. One is Table format F(s, d), data measured from bead on plate. There are four equations derived based on certain assumptions on heat transfer, such as Hannerz Equation, Rykalin 2D and 3D equations, Rosenthal Equations. The accuracy of this programs are very poor, the previews trials results are proved the same.

2.5.4 Quicksim

The Gleeble® system has a full set of software tools. The operator can generate tests on the work station through a number of programming options, including QuickSim software, a spreadsheet-like, a windows based software, this program is used to generate tables for hot deformation system, Heat Affected Zone and Gleeble® Script Language (GSL) files to run the machine that describes each action in a test sequence in order and duration. It allows arbitrary programming of waveforms for both thermal and mechanical systems.

For this present work table format is used to enter the data's acquired from the sysweld software and successfully runned.

2.5.5 Specimen Preparation

A specimen dimension of 86×11×11 (all in mm) had been prepared with smooth finish on the surface which can be used for the following test

1. Charpy impact test
2. Hot ductility test / Tensile test
3. Microstructure / Micro-hardness test

Chapter - 3

Results and Discussion

Grade 92, a high chromoium and tungsten material experience differentness in welding metallurgy during welding as of HAZ region. Their comparison of microstructures and mechanical properties are multifaceted and changeable. Hence, assessment on the evolution of microstructure and its mechanical properties of these areas (HAZs) are necessary to evaluate the weldability of the base material.

3.1 Macrostructural Analysis of Weld

After welding, radiography methods of non-destructive examination (NDE) for welded samples were carried out to find presence of any discontinuities during the course of welding. The samples were free from discontinuities during welding as it is evident from below figure 3.1.Macro-etching by Vilella's reagent of 1 gm of picric acid, 5 ml of HCL and 100 ml of ethanol/methanol was prepared and etched for a longer duration of 6-8 mins for macrostructural analysis under stereo microscope. Figure 3.1 shows macrograph of as weld samples showing complete penetration and fusion all along the welding layers and passes.

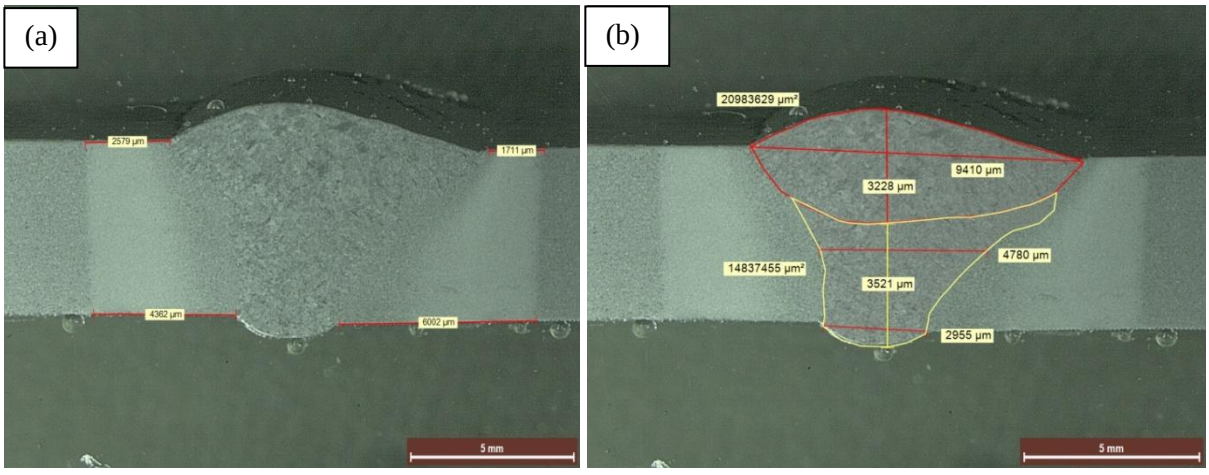

Figure 3.1 Transverse View of Welded Specimen Macrostructure at same place.

The macrostructure had been analysed for number of passes, defects, penetration, fusion between base metal and weldment. The length and width of each pass of weld metal deposit and Heat Affected Zone (HAZ) were numerically evaluated. Due to oscillation, there are possibilities for non-alignment of centre line between V-groove and welding torch which resulted in difference of HAZ width largely so it has been approximated as the width of Top

as 2.579 mm and Bottom as 4.362 mm which was then compared for computer modelling by sysweld.

3.2 Weldment Analysis

Non destructive Radiographic analysis for optimised condition had been performed on the welded specimen where found to be free from discontinuities/weld defects compiled with standard ASME Section-9: Qualification of weld.

3.2.1 Microstructure Analysis

Several welding trails has been carried out on P92 steel to optimise the input current, preheat temperature ranging from room temperature to 300 °C, travelling speed, gas flow rate and post weld heat treatment and overall heat energy. Finally the optimised heat input was 819 J/mm for 1st pass and 841 J/mm for 2nd pass. Microstructure in as-welded condition reveals lathe-type martensitic structure by etchant, Vilella's reagent for 1-3 mins and had been compared for delta (δ) ferrite presence as in figure in 3.2 that deteriorates the weld quality. With all the trails commonly found to have significant quantity of delta ferrite at all the heat input and also for retained austenite. After PWHT the microstructure shows mainly acicular form of ferrite and widmanstatten ferritic structure along with tempered martensite in it. The retained austenite and delta ferrite in the weldment during PWHT will transform in upper and lower bainitic structure i.e. carbides and cementite particles in ferrite matrix [27].

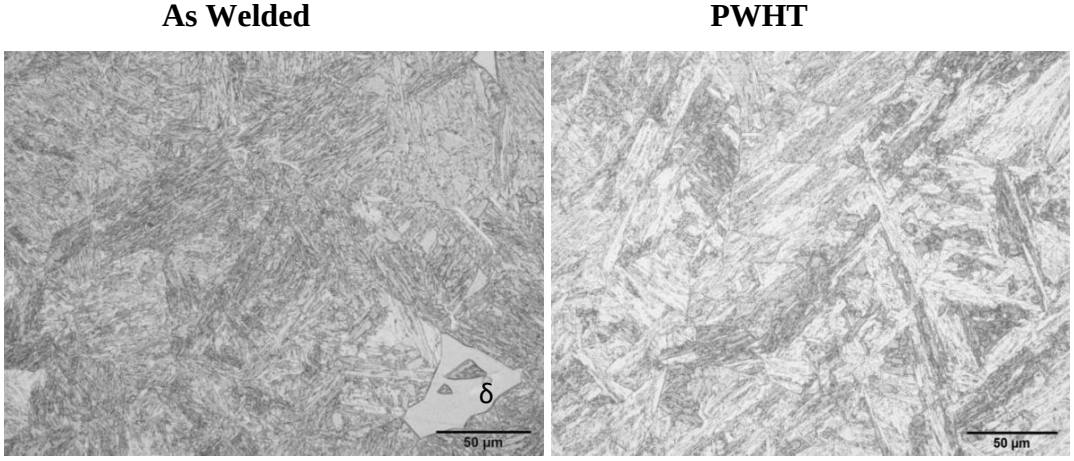

Figure 3.2 Microstructure of weld.

3.2.2 Micro-Hardness Analysis

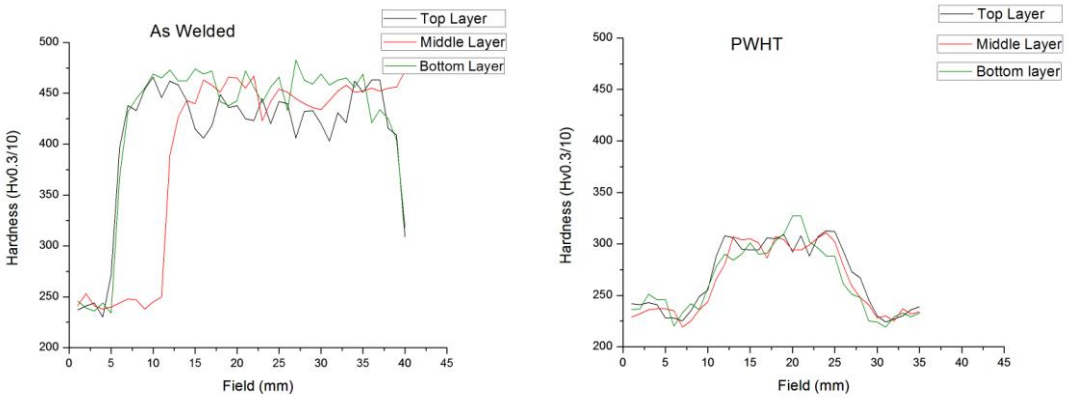

Figure 3.3 Hardness profile comparison.

Hardness has been analysed for this optimised heat input in as-welded and heat treated condition which falls in the allowable limit according to the standards and manufactures suggested. The highest hardness from figure 3.3 in the weld region is mainly attributed to delta ferrite presence, which has been reduced during the post weld heat treatment by transforming in to tempered martensitic/bainitic structure. The HAZs hardness was higher than BM, due to the presence of quenched martensite in HAZ and tempered martensite in BM. The quenched martensite and tempered martensite are composed in ICHAZ so hardness is between that of FGHAZ and BM [28 - 30].

Due to presence of large amount of ferrite stabilizing element like chromium tungsten and molybdenum, during heat treatment the BCT crystal structure of martensite has been transformed in tempered bainite i.e. a type of BCC iron ferrite with finely dispersed carbide cementite particles in it formed along the prior austenite grain boundaries which shows reduction in the hardness profile [10, 11].

3.2.3 Weld Toughness Analysis

Fracture toughness of metal strongly depends on the microstructure which was carried out by Charpy V-Notch (CVN) technique on subsize samples which was then compared with the European specification BS EN 1599:1997 shows that toughness value requires a minimum average value of 47 J and a minimum single value of 38 J at +20 °C where as the obtained result for the following electrode EN12070 (12CrMoV) with optimised welding parameters was 32 J on an average and 20 J of single value i.e. brittle as evidenced by its fracture surface from figure 3.4, which can be increased further by increment in Preheat temperature but the

Charpy values specified by P92 manufacture for a well-established weld metal BS EN12070 (12CrMoV) should require 34 J on an average and 22 J of minimum single value at +20 °C [10].

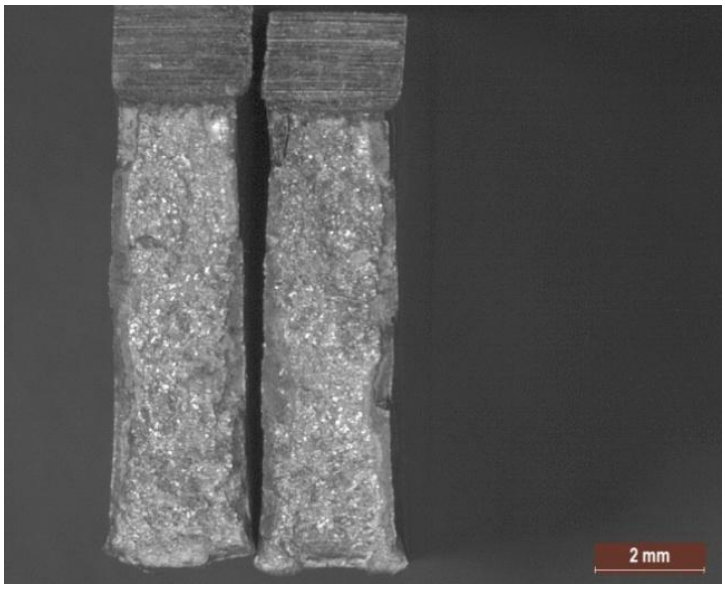

Figure 3.4 Brittle fracture of weld metal.

3.2.4 Tensile Test Analysis

Transverse reduced rectangular section tension specimens for pipe has been prepared and analysed for the fracture region according to the standard AWS B4.0 and ASTM designation E8. The result shows that weld metal is more brittle followed by HAZ and being the failure region was in base metal as shown in figure 3.5 and the ultimate tensile strength (U.T.S), Yield strength (Y.S), percentage of Elongation (%E), percentage of reduction in area (%RA) has shown in below table 3.3.

Table 3.1 Tensile test result.

Description	Evaluated Values
Ultimate Tensile Strength (U.T.S) MPa	739
Yeild Strength (Y.S) MPa	596
Percentage of Elongation (%E)	17
Percentage of reduction in area (%RA)	55

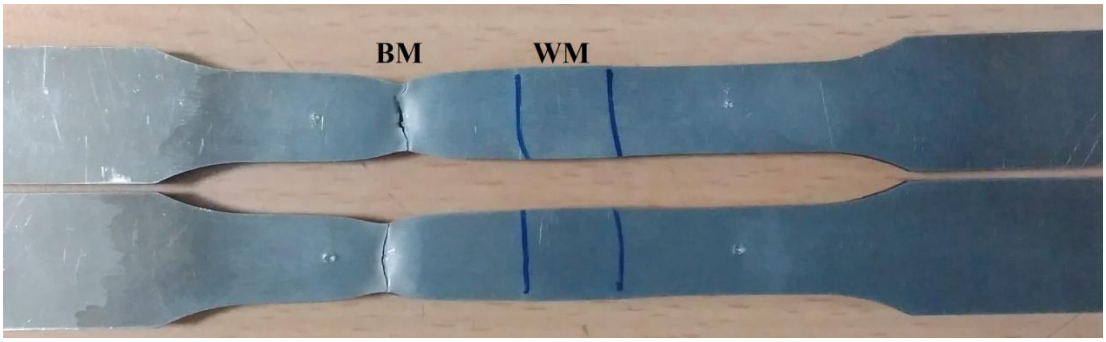

Figure 3.5 Tensile test specimens.

3.2.5 Bend Test Analysis

To check the ductility of the welded joint bend test was carried out which is evidenced by its ability to resist tearing and the presence of defects on the tension surface according to standard AWS B4.0. The face and root bend test was carried on a 3 mm thick transverse section specimen for the weldment to an angle of 180°. It has been observed that there was no micro-fissure tearing or defect opening on the root side but on the face side after 24 hours of relaxing time it was observed a crack size of 5.2 mm had developed in the HAZ region as shown in figure 3.6. This is probably due to relaxation of strain energy in the brittle martensitic structure of HAZ.

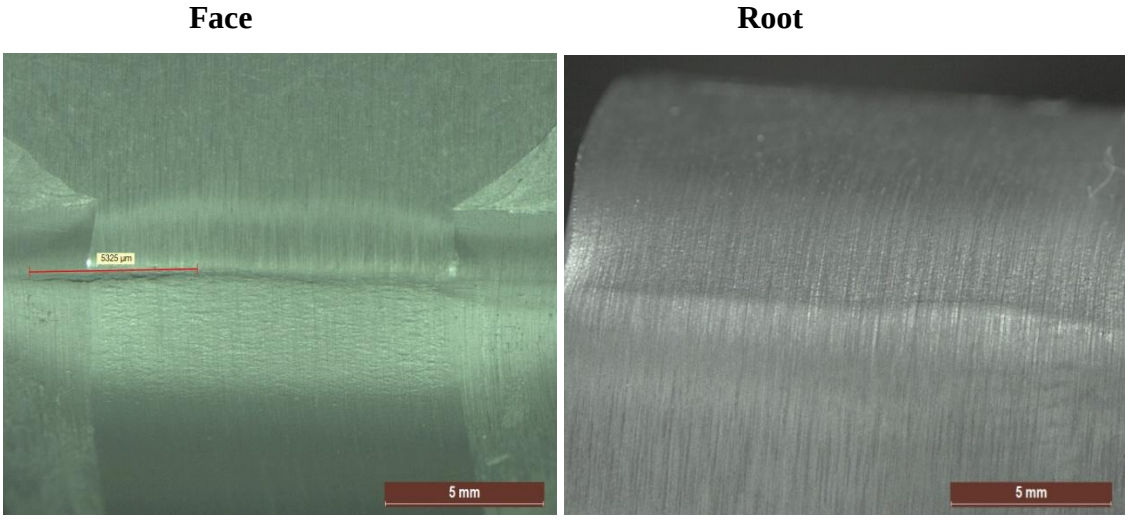

Figure 3.6 Bend test macrostructure.

3.3 Sysweld Simulation Analysis

Sysweld software simulation of the welding process which used double ellipsoid heat source model is standardized for weld thermal cycle along with the input of optimised welding

parameters, materials properties such as thermal conductivity, density, specific heat, thermal expansion coefficient, elastic modulus, yield strength and poisson's ratio to the software and compared with the weld profiles between the simulation and the experimental bead profiles such as length (L) and width (W) of weldment and HAZ, convexity of top and bottom bead. It has been found that actual input of heat energy in real weld and heat energy need for simulation with sysweld varies by 25% which is higher for sysweld, to cover the melting temperature for the whole bead to fusion line of each pass, which can be attributed towards the oscillation of welding torch efficiency.

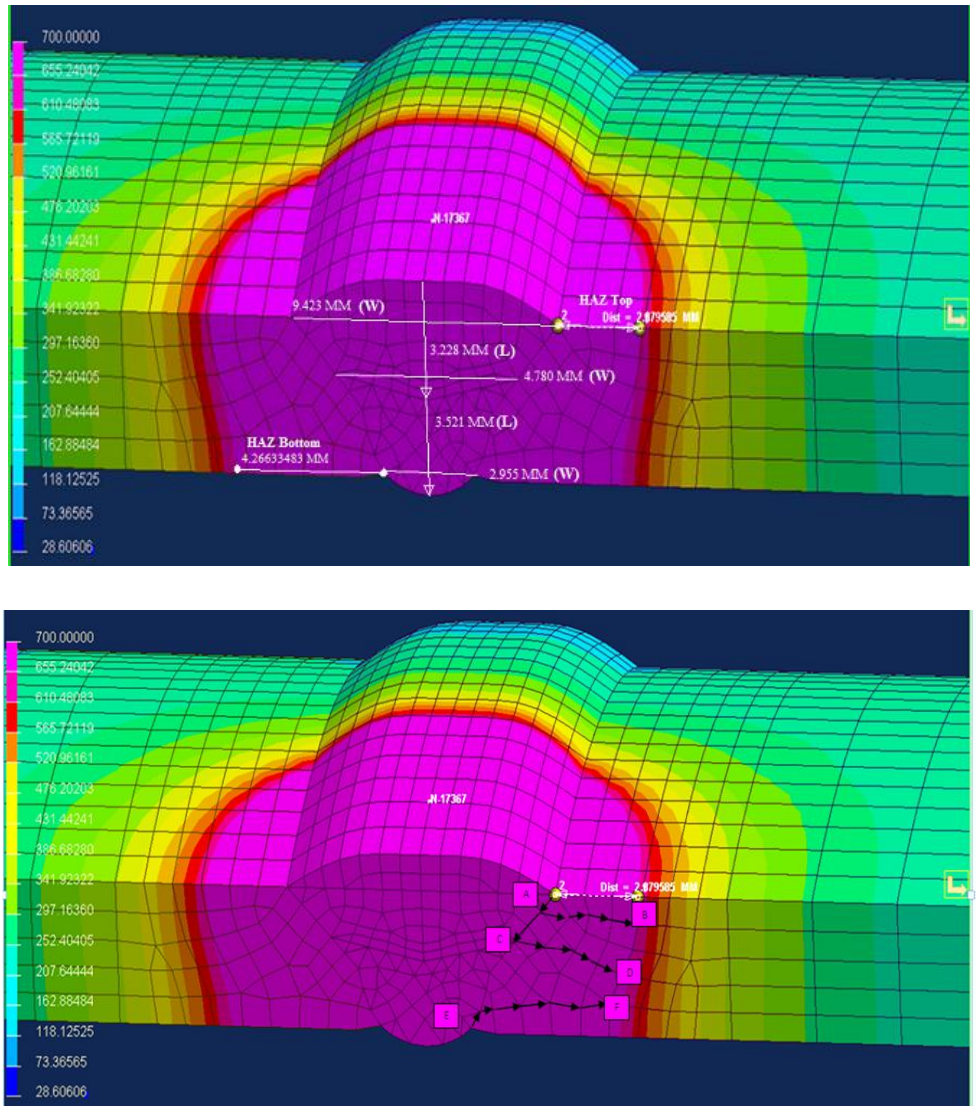

A ⟶ **B** – 0.67 mm from top (X), from X - 1.067 mm, 0.652 mm, 0.812 mm, 0.89 mm.

C ⟶ **D** – 0.47 mm from X - 0.88 mm, 1 mm, 2.4 mm.

E ⟶ **F** – 0.64 mm from bottom (Y), from Y - (0.45, 0.85) (1.42, 1.01) (1.02, 1.14) mm.

Figure 3.7 Sysweld simulation of weld thermal cycle.

The simulated weld and HAZ where in well accordance with the real weld and HAZ which had been compared numerically from macrostructure of the HAZ and simulated HAZ of the sysweld in table 3.2 and also depth and width of weld pool as shown in figure 3.7.

Table 3.2 Comparison of HAZs.

Details of HAZ	Width (mm)	
	As welded	As Simulated
Top	2.57	2.87
Bottom	4.32	4.26

The positions of monitoring points are shown above, each strip are designated as Top A-B, Middle C-D, bottom E-F and colour coding represents the respective temperature field and thermal gradient of the material from melting point to room temperature. The points mentioned above are selected for weld thermal cycle's simulation from sysweld which covers over a wide range of temperatures from 1330 to 500 °C. The simulated welding thermal cycle curves were pulled out from the established double ellipsoid welding heat source model. The output data's of sysweld as weld thermal cycles was the input for physical simulator-Gleeble, so the large no of data's had been trimmed down by Web Plot Digitalizer software version 3.7 to lessen the length of program.

3. 4 Heat Affected Zone Analysis

Using the thermal cycle generated by Sysweld software, a Quicksim program can be generated associated with Gleeble. The Quicksim program can be modified further, when necessary, before running the test. Microstructure and hardness of simulated double bead thermal cycle of the weld at various locations of different peak temperature has been compared with microstructure of as welded and post weld heat treated are as follows. From the thermal cycle figures it is evident that inter-pass temperature has been maintained at 200 °C and interpass time as 80 seconds.

Table 3.3 Peak temperatures and hardness comparison chart.

Peak Temperature °C	**Without PWHT** (HV0.3/10)		**PWHT** (HV0.3/10)		**Impact Toughness Energy (joules)**
	Welded	**Simulated**	**Welded**	**Simulated**	
1 - 690/1204	463	374	350	499	199
2 - 652/1089	416	493	293	440	181
3 - 612/970	409	427	273	320	184
4 - 567/872	320	370	267	290	162
5 - 957/1330	466	532	311	357	45
6 - 718/1122	463	528	302	330	142
7 - 662/1013	443	515	289	335	186
8 - 1362/1310	433	514	327	381	49
9 - 1265/1293	483	506	302	337	80
10 - 1060/1229	459	430	288	370	192
11 - 878/1148	466	523	261	435	92

3.4.1 HAZ Micro-Hardness correlation

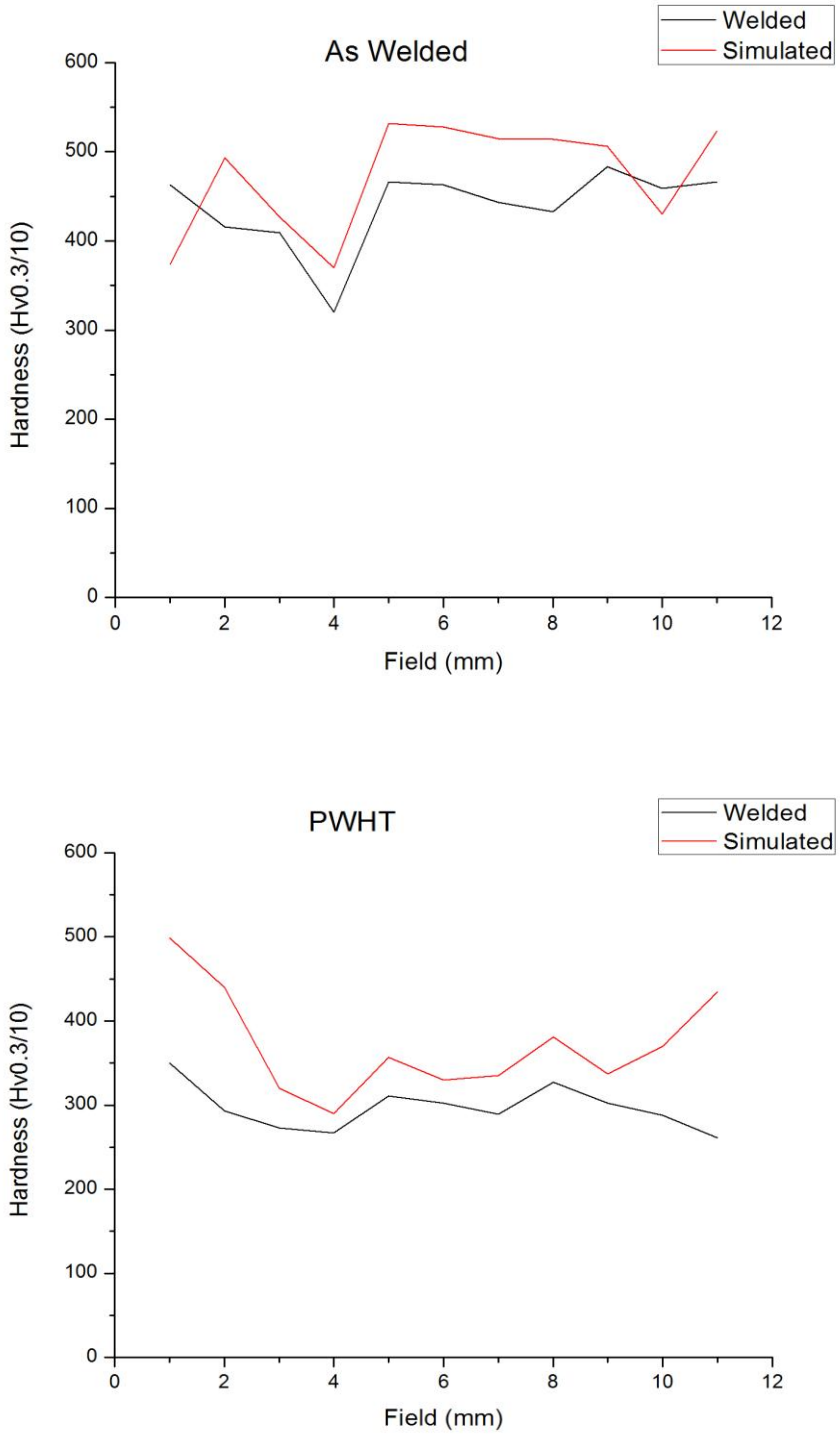

Figure 3.8 Hardness comparisons for simulated and real time HAZs.

Figure 3.8 shows the variation of hardness in the real time and simulated heat affected zone (HAZ) which has been discussed with microstructure below. Field represents region 1-11.

3.4.2 Thermal Cycle and Microstructure Comparison

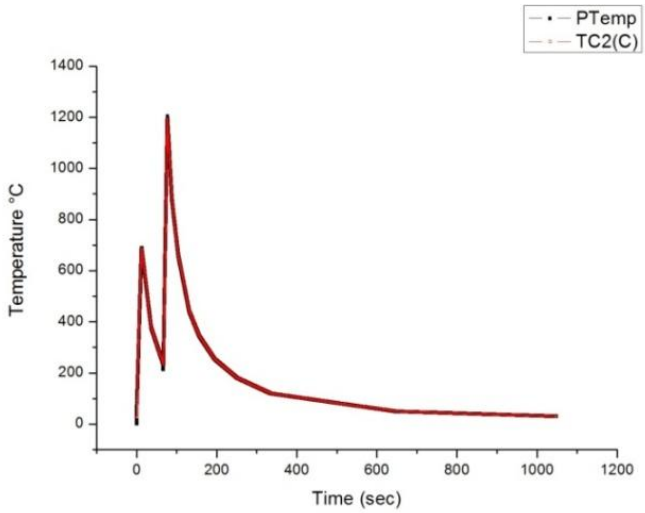

Welded **Simulated**

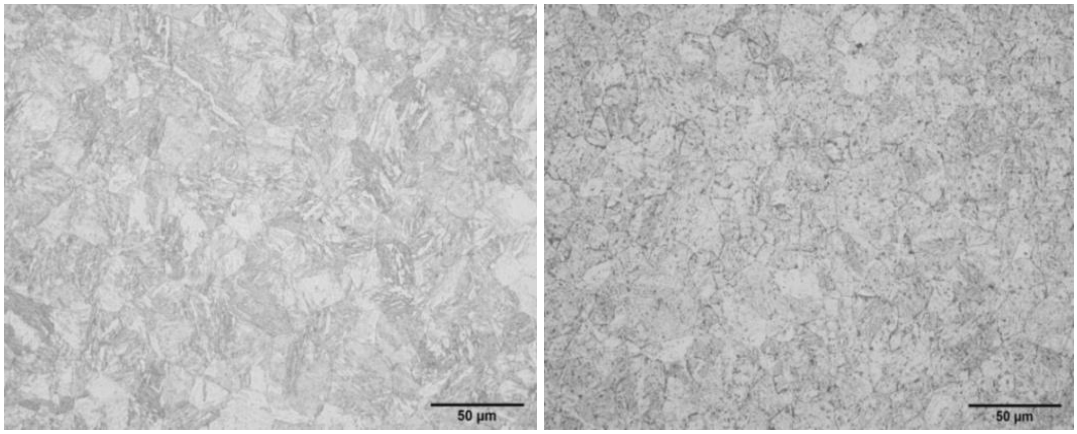

PWHT

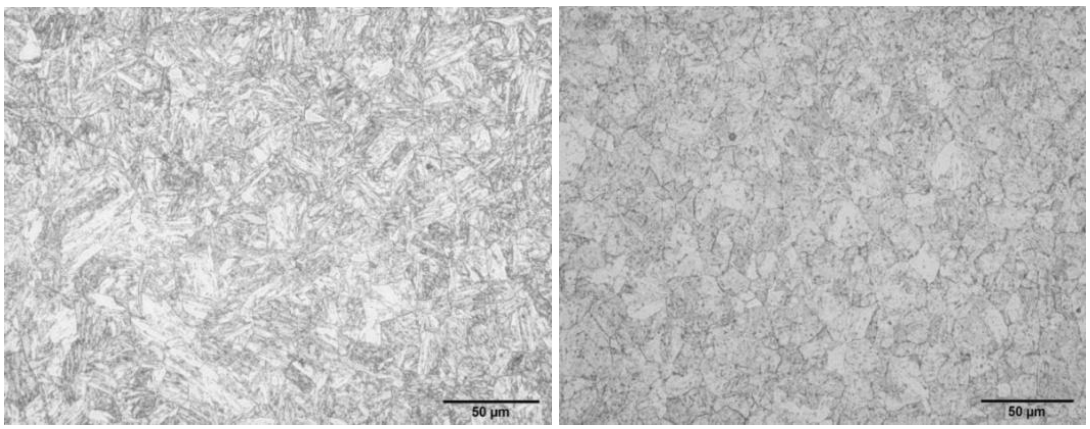

1. Top-1.067 mm (690/1204 °C).

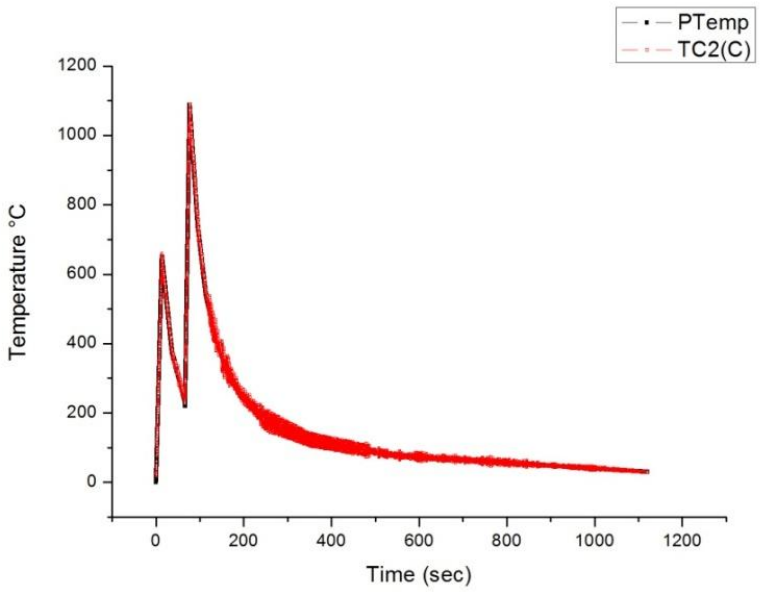

Welded **Simulated**

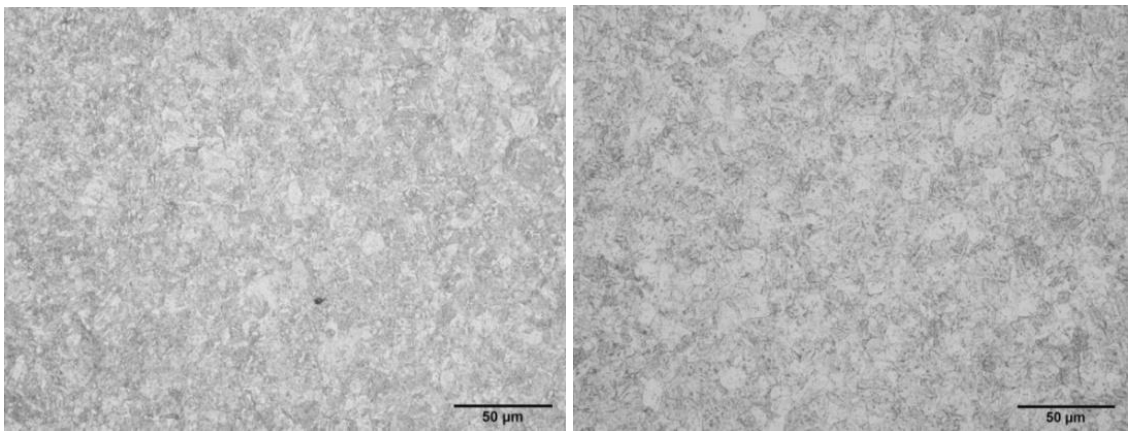

PWHT

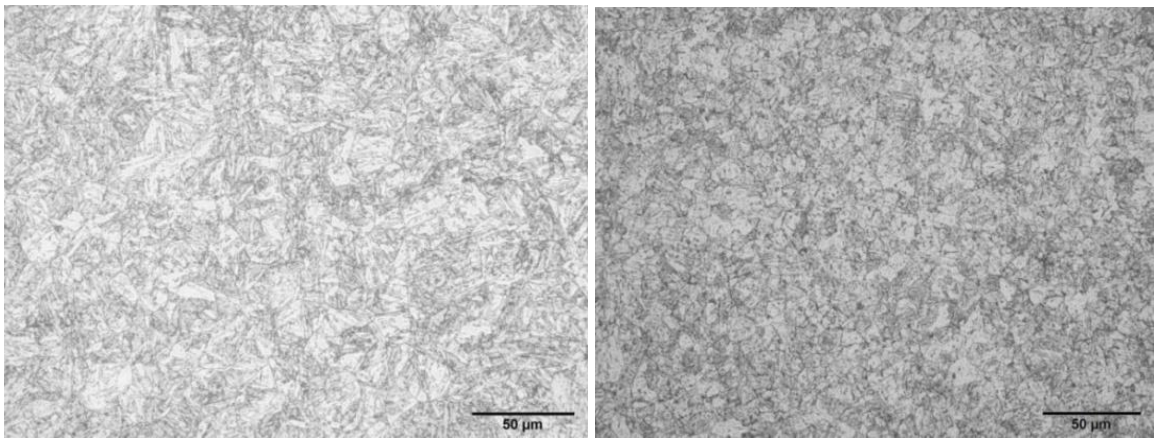

2. Top-0.652 mm (652/1089 °C).

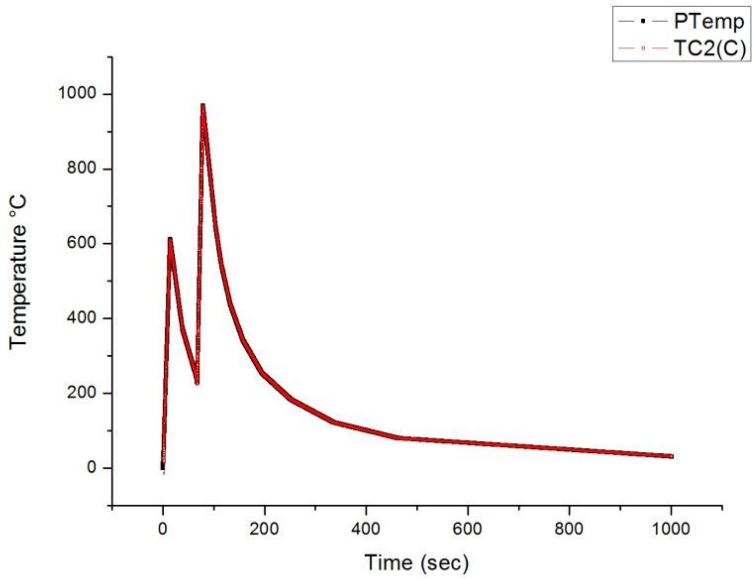

Welded **Simulated**

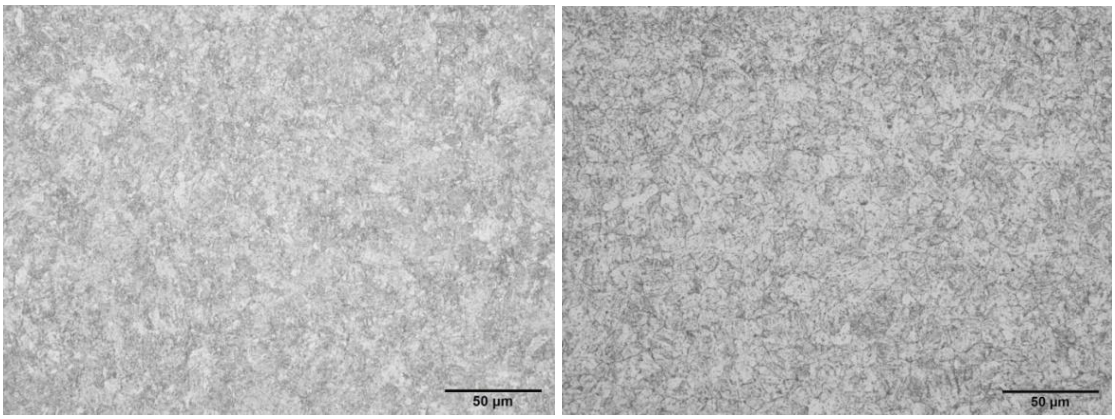

PWHT

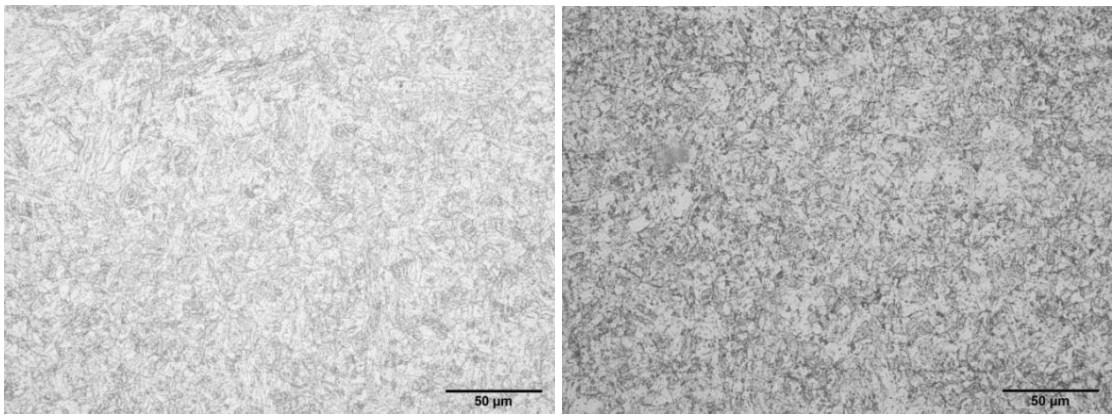

3. Top-0.812 mm (612/970 °C).

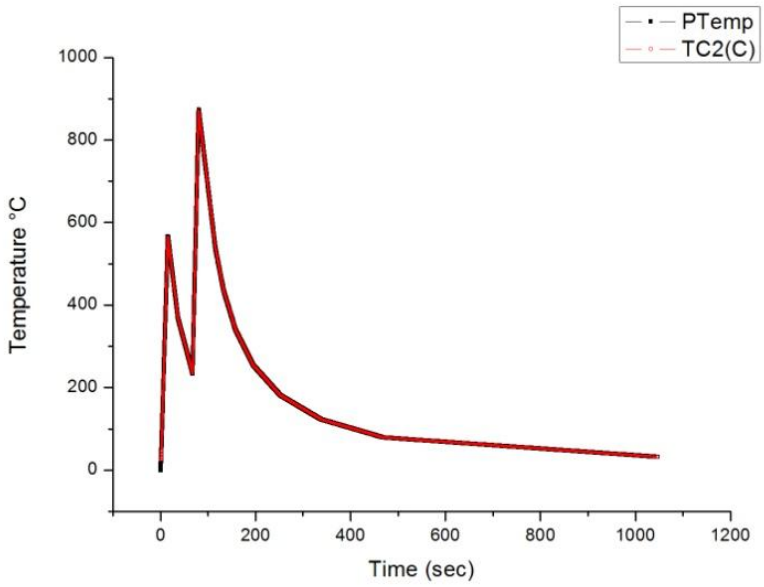

Welded **Simulated**

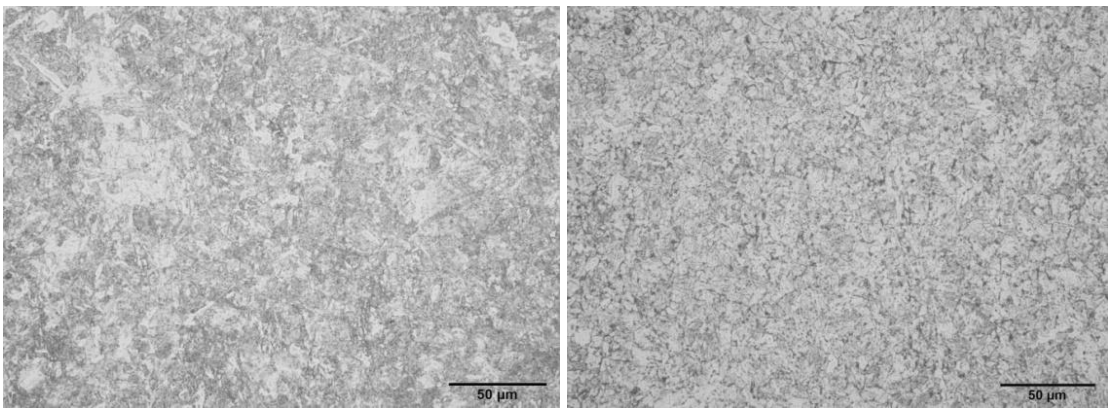

PWHT

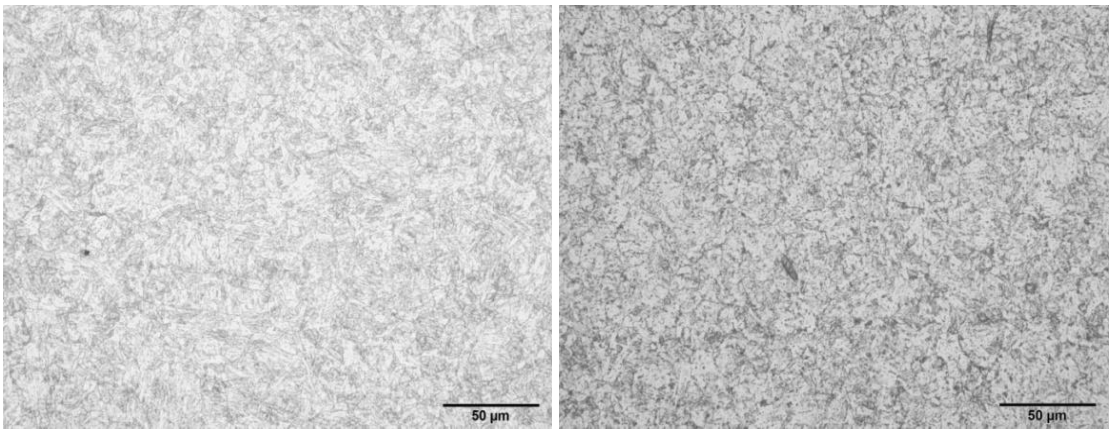

4. Top-0.89 mm (567/872 °C).

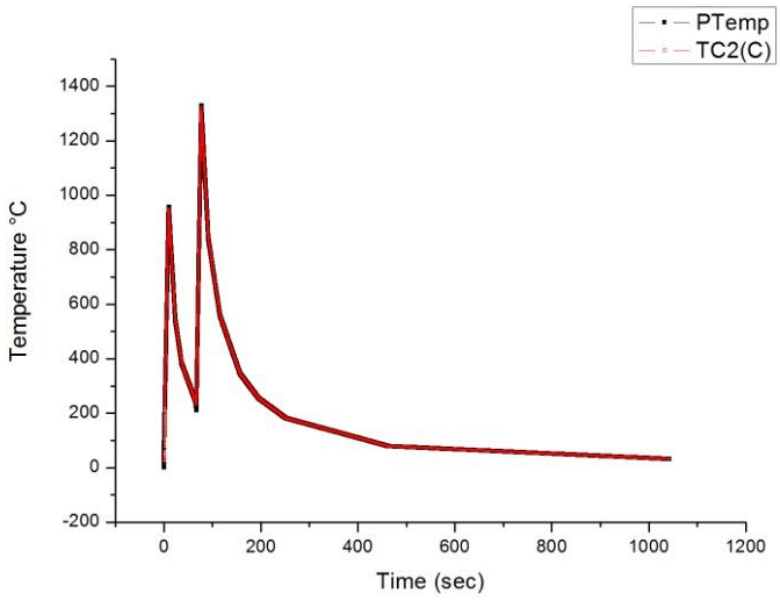

Welded **Simulated**

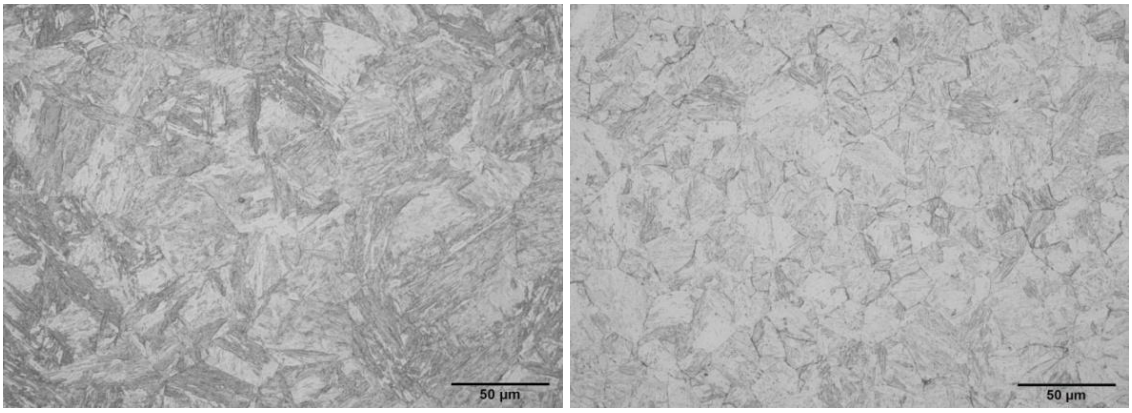

PWHT

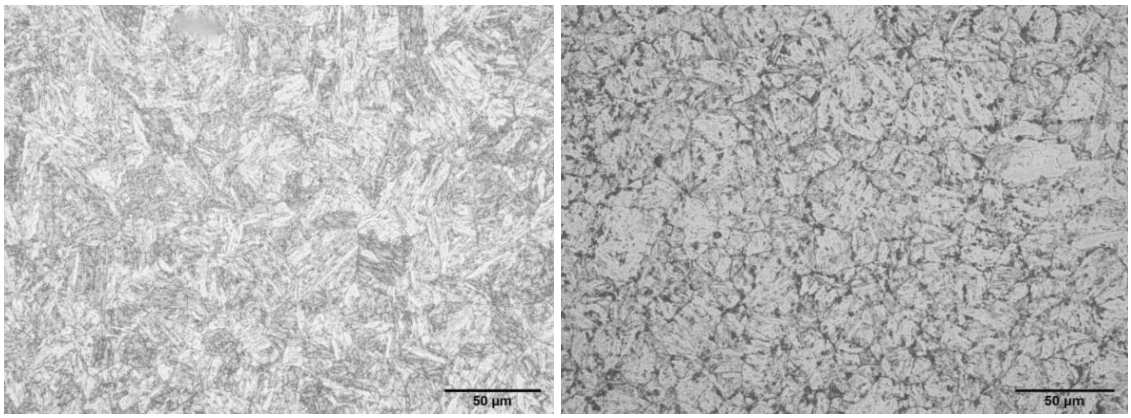

5. Middle-0.88 mm (957/1330 °C).

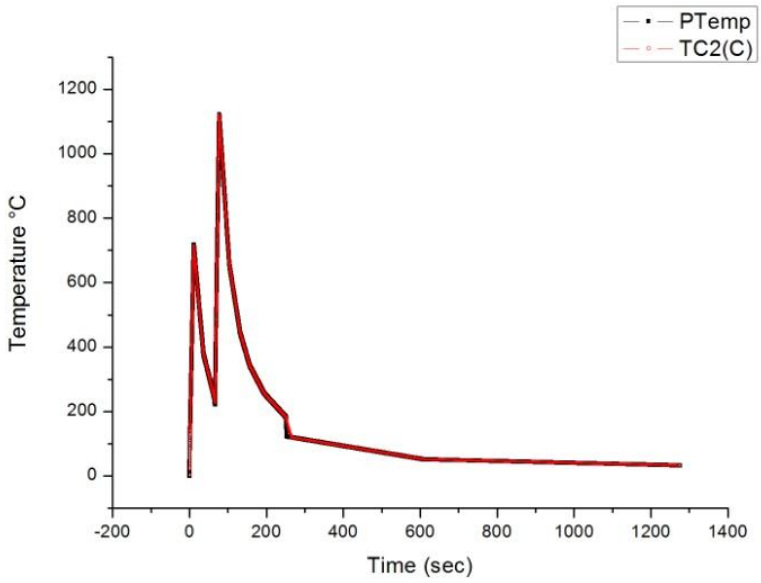

Welded **Simulated**

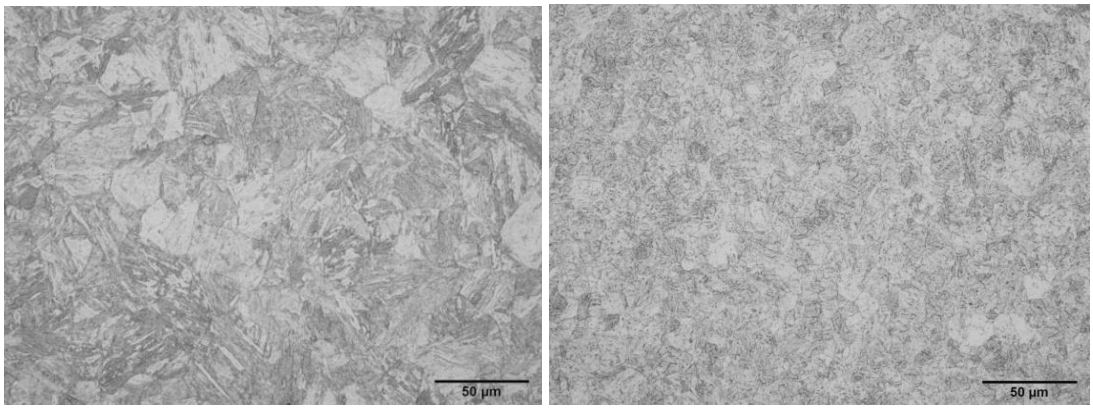

PWHT

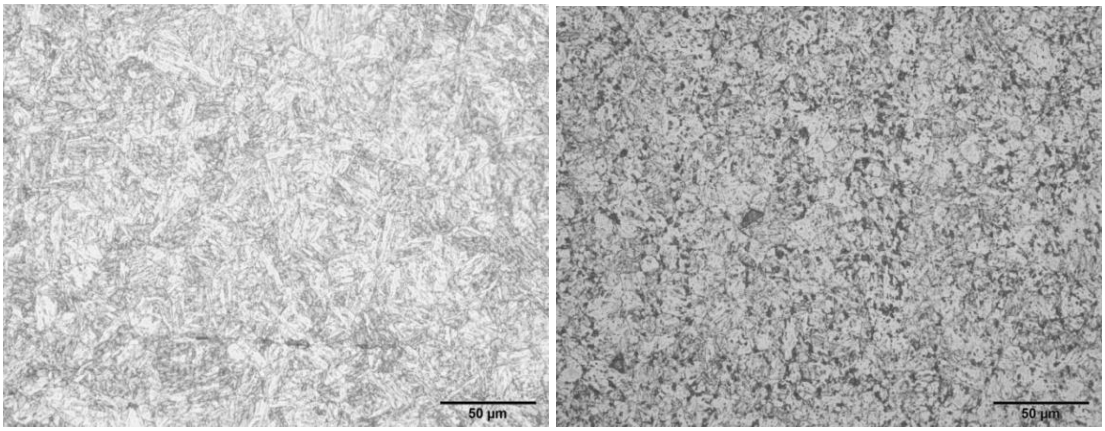

6. Middle-1 mm (718/1122 °C).

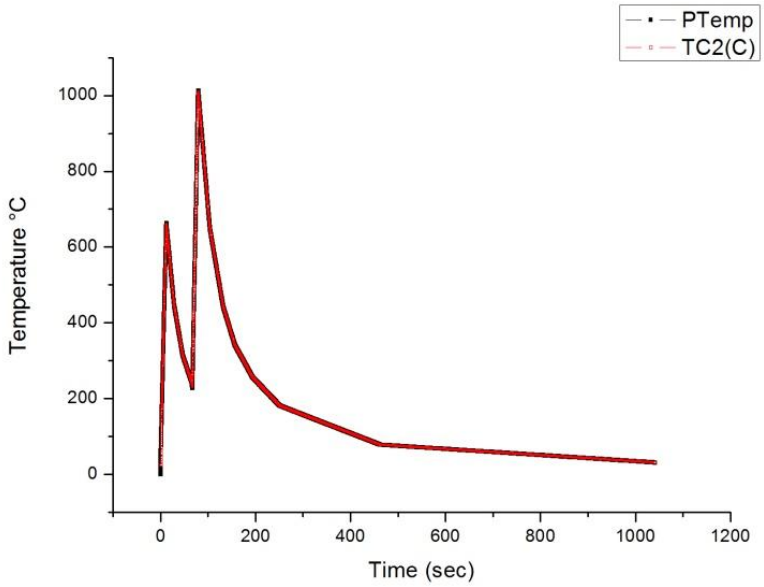

Welded **Simulated**

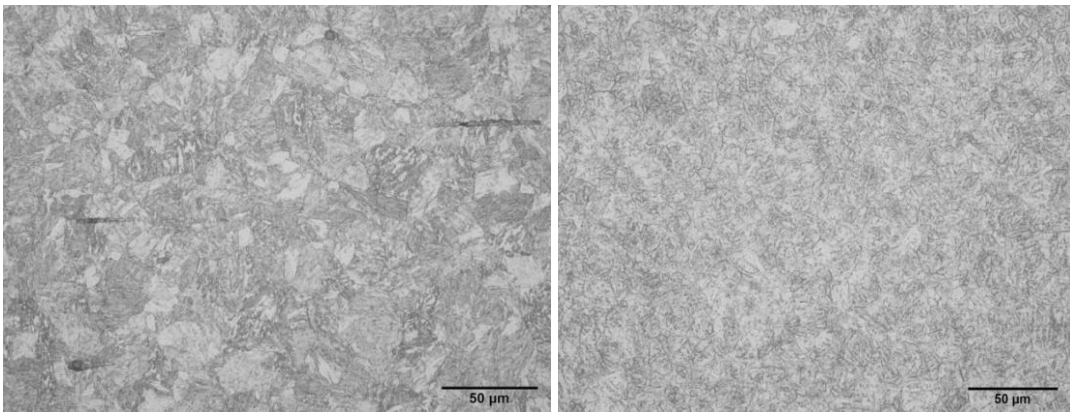

PWHT

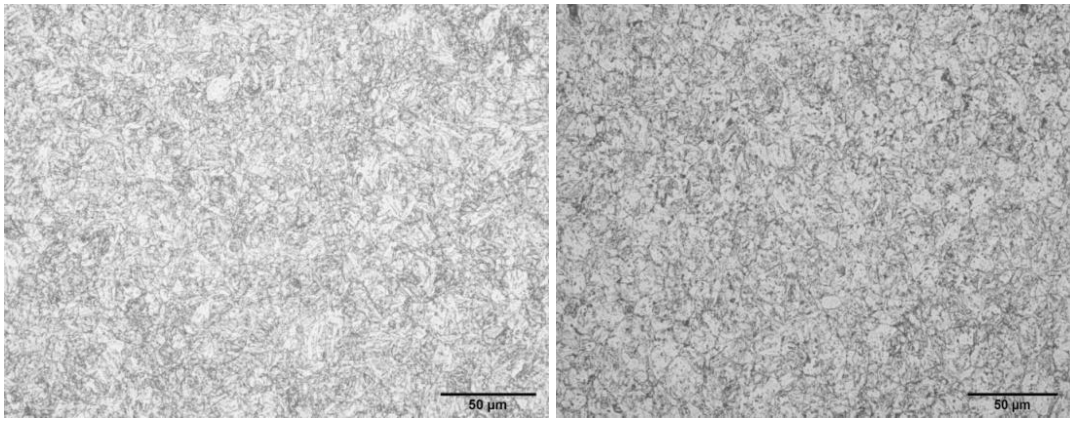

7. Middle-2.4 mm (662/1013 °C).

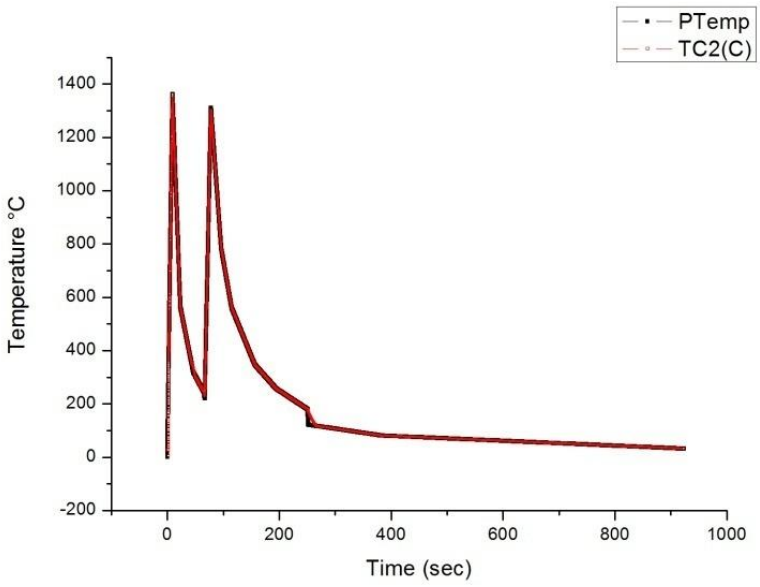

Welded **Simulated**

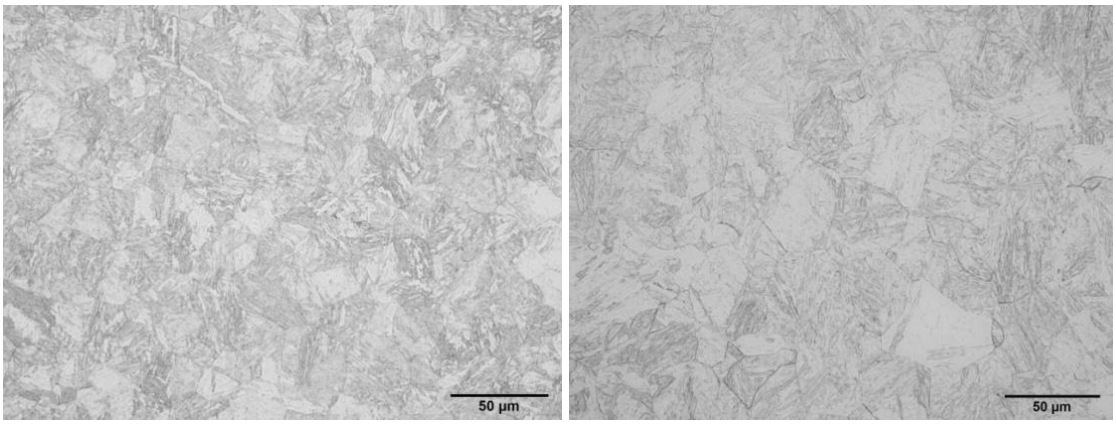

PWHT

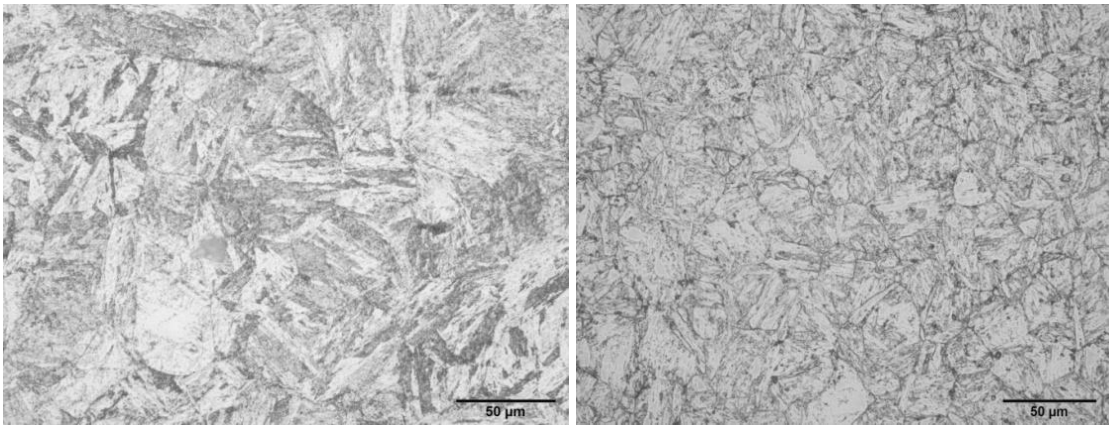

8. Bottom-0.64 mm along fusion line (1362/1310 °C).

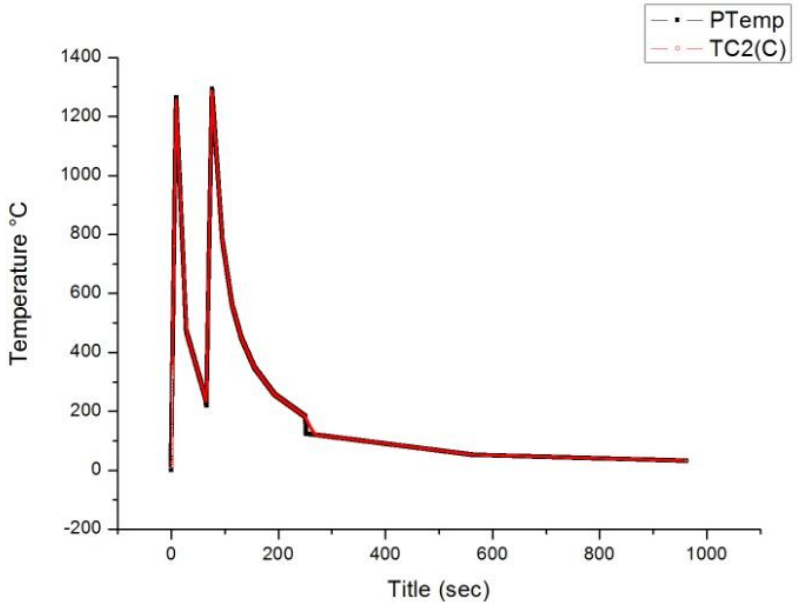

Welded **Simulated**

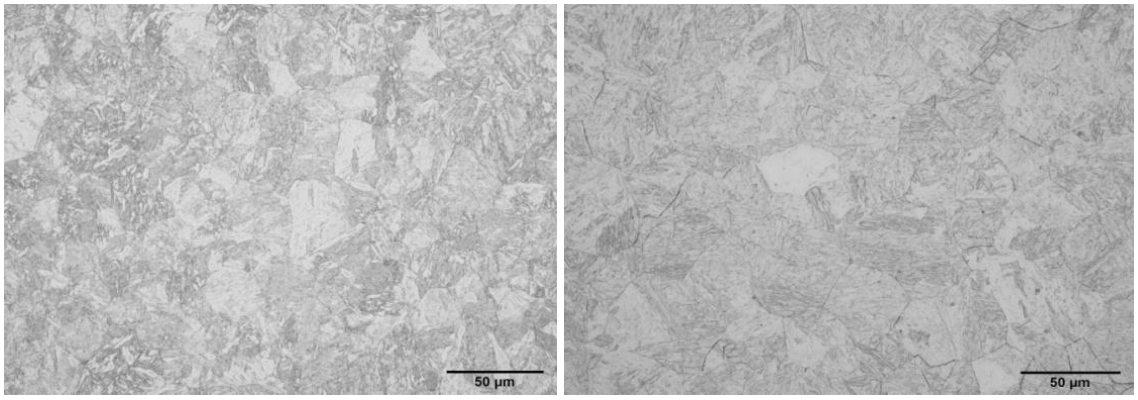

PWHT

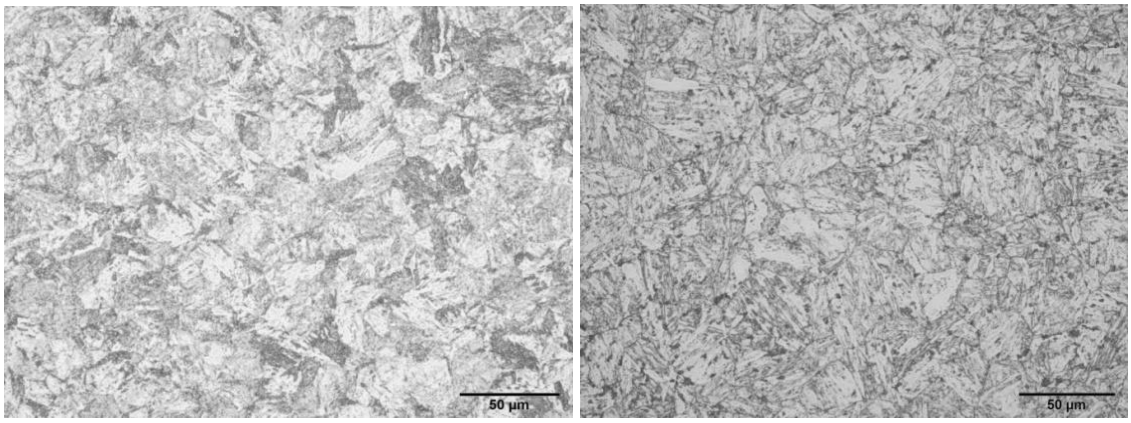

9. Bottom-0.45, 0.85 mm (1265/1293 °C).

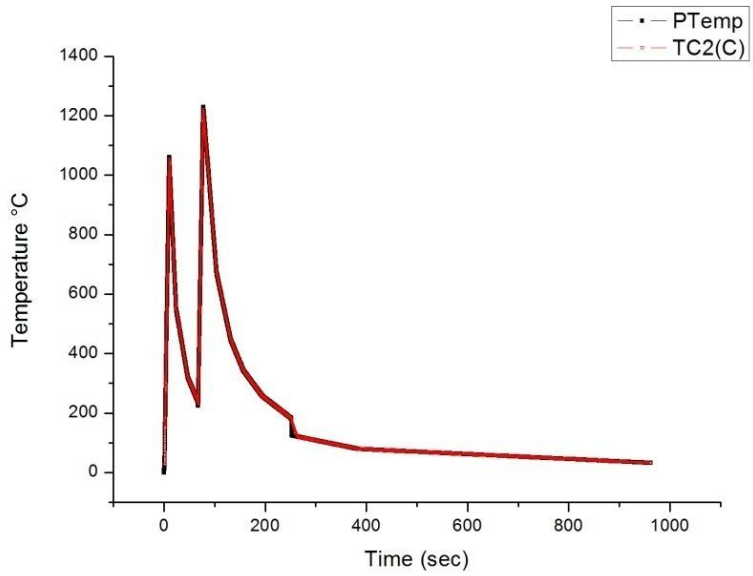

Welded **Simulated**

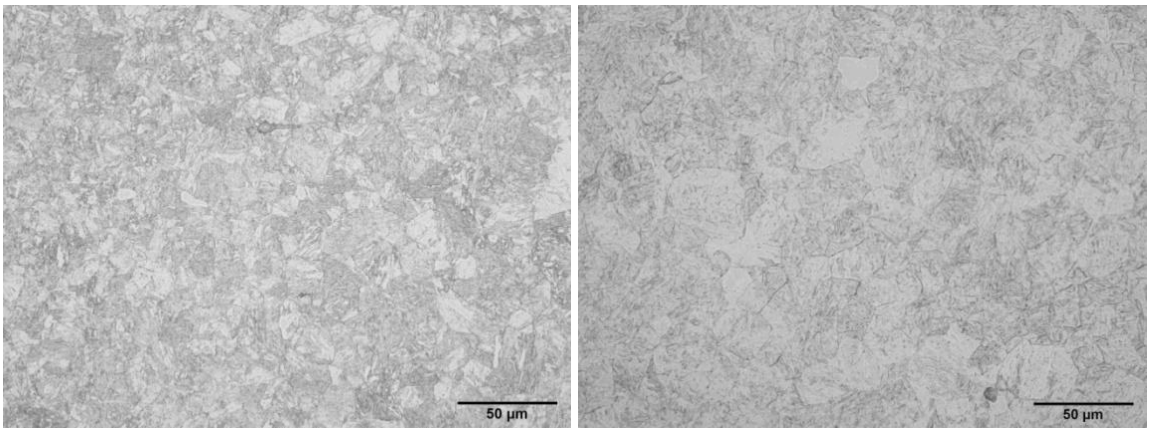

PWHT

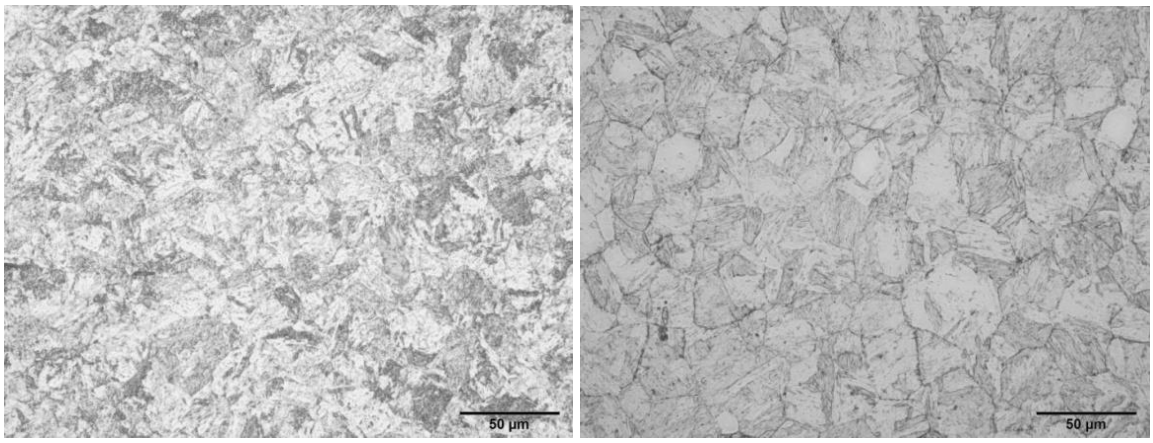

10. Bottom-1.42, 1.01 mm (1060/1229 °C).

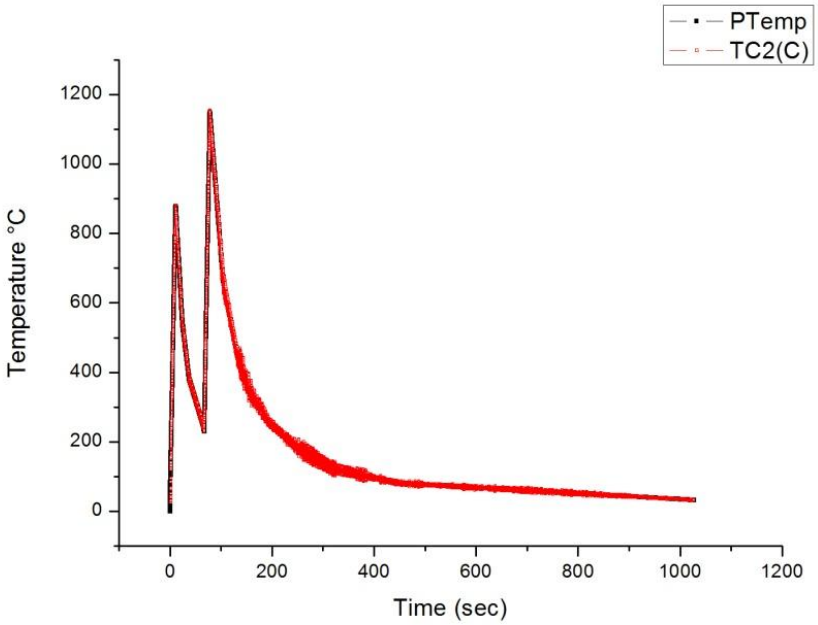

Welded **Simulated**

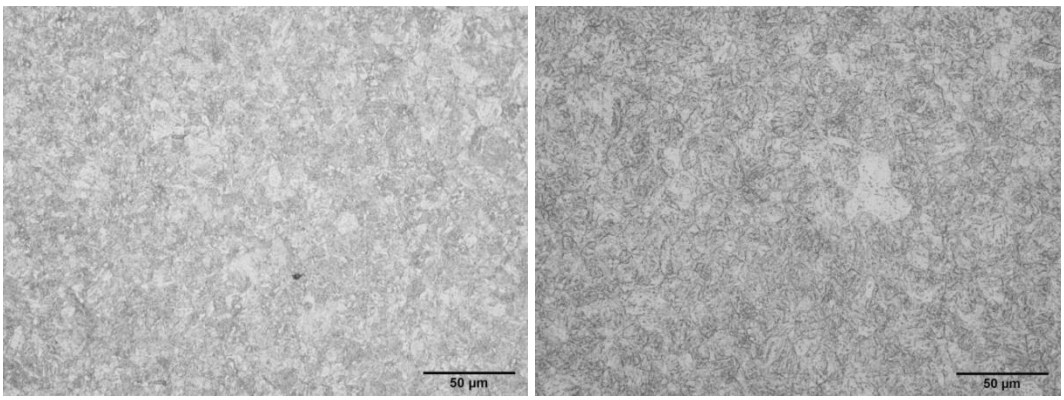

PWHT

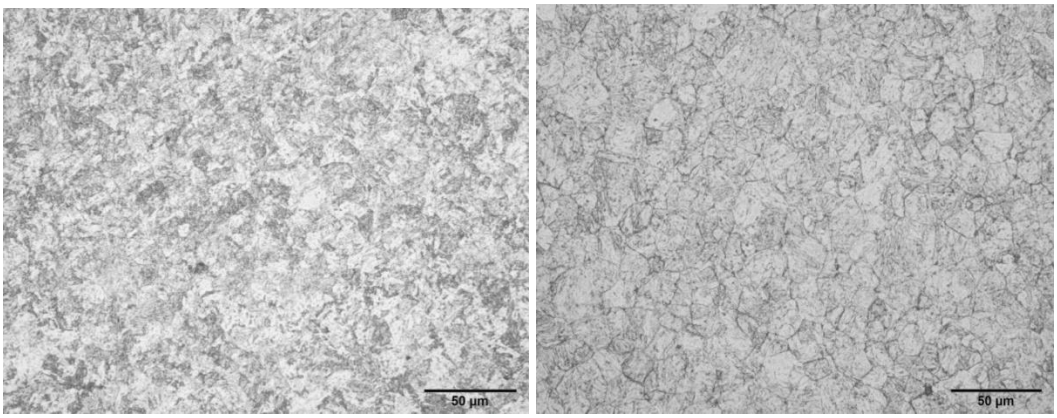

11. Bottom-1.02, 1.14 mm (878/1148 °C).

Figure 3.9 Region 1 to 11- simulated weld thermal cycle and microstructure.

***Note** Regions mentioned with scale with as preceding point as starting point in mm

When the carbon content is 0.07-0.13%, the BM has dual phase microstructures with tempered martensite and thin strips of delta (δ) ferrite or α ferrite while in the areas of HAZs, the microstructural evolution is complex to justify which is governed by chemical compositions and cooling rates. The maximum cooling rate to form ferrite was 0.1 °C/s for P92 steel. When the cooling rates upto 20 °C/s had bainitic transformation and above martensitic transformations were achieved and cooling rates above 20 °C/s had little influence on the microstructure and micro-hardness of martensite [10].

Physically simulated HAZ and Real time HAZ had been compared with their microstructures and Hardness values. The comparative results in the table 3.3 and figure 3.8 and 3.9, shows that there has been a variation in Vickers micro-hardness values which range from 15 to 10%. The microstructural comparison of the as welded and simulated and also with heat treated at 760 °C for 30 mins has shown that no significant correlation between microstructures at large variation in hardness.

The microstructure of coarse grain HAZ (CGHAZ) as-simulated for the temperature range 1122-1293 °C simulated show irregular shaped prior austenite grains, sizes of few microns as shown in region-1, 6, 9 & 10 where as in the real time HAZ it has high martensitic character with prior austenitic grain boundaries. This difference made there has been considerable variation in the hardness of ~20%, even in region-6 it shows more retained austenite and thin delta ferrite in the as welded condition but not in simulated at the fastest cooling rate. In region-1 without PWHT it shows major variation of 100HV and with PWHT it shows 200HV.

Fine grain HAZ (FGHAZ) region where the peak temperature experienced above A_{c3} i.e. 950-1100 °C has completely quenched martensitic in character with few prior austenite grains visible in region-2 & 3, where as in simulated, fine grains of random shapes are visible. As in region-7 the peak temperature was 1013 °C due lateral high heat input, it shows high quantity of retained austenite and prior austenite grains, at even 2.4 mm far from the fusion line at the mid range in as-welded condition where the hardness has a variation of 50HV both in simulated and heat treated in comparison with real time. From region-11 it has experienced a peak temperature of 1148 °C in grain growth region for CGHAZ shows a hardness variation of 60HV without PWHT, after PWHT it has shown grain growth but hardness has not been reduced and this FGHAZ is the region of higher creep rate than other regions in HAZ.

Inter-Critical HAZ region, which experienced a peak temperature in between A_{c1} and A_{c3} where the peak temperature was 872 °C that correspond to region-4. The resultant microstructure shows different forms of ferrite and lath martensite, which also includes tempered martensite, newly formed quenched martensite, and thin strip δ-Fe in the as-welded condition where as in simulated it shows formation of tempered grains at experimental temperature of 870 °C. In the PWHT condition, the real time HAZ shows tempered bainite where as in simulated, shows overtempered, when compared hardness without PWHT it shows 50HV variation where as in PWHT it shows 30HV.

The region which experienced temperature above 1300 °C contains big-blocky delta ferrite i.e. diffusion controlled phase on cooling, so it will not have sufficient time to complete the phase transformation process from δ-Fe to γ-Fe and then to martensite due to high cooling rate in GTAW, the original δ-Fe in the BM grows quickly and combined at this high temperature range and also a network of Martensite-Austenite islands along prior austenite grains observable from region-8 and 5 in without PWHT condition. It is evident from microstructure that grains in this region are coarser with lath type martensite in the real time HAZ, but in correlation, simulated microstructure shows grain size variation. Hardness comparison without PWHT shows 75HV variation where as with PWHT, it shows upper bainitic structure with 65HV variation [30].

3.4.3 Fracture Toughness

Charpy V-Notch (CVN) test for post weld heat treated samples had been evaluated for simulated samples that are listed in table 3.3 in correspondence with temperature. Region of various peak temperature shows no correlation of impact energy with respect to hardness, as high hardness should result in low fracture toughness energy but region-1 has absorbed more energy of 199 joules that correspond to shear fracture where fracture surfaces are shown in figure 3.10, for peak temperature around1300 °C, it shows brittle fracture with absorbed energy of 45 joules where fracture surface is shown in figure 3.11.

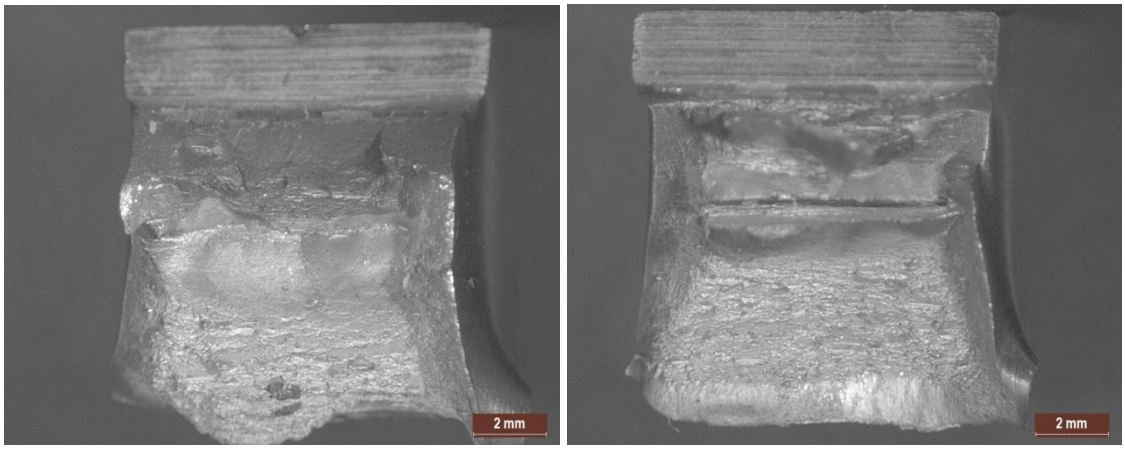

Figure 3.10 Shear fracture of simulated samples-Peak Temperature of 1060/1229 °C.

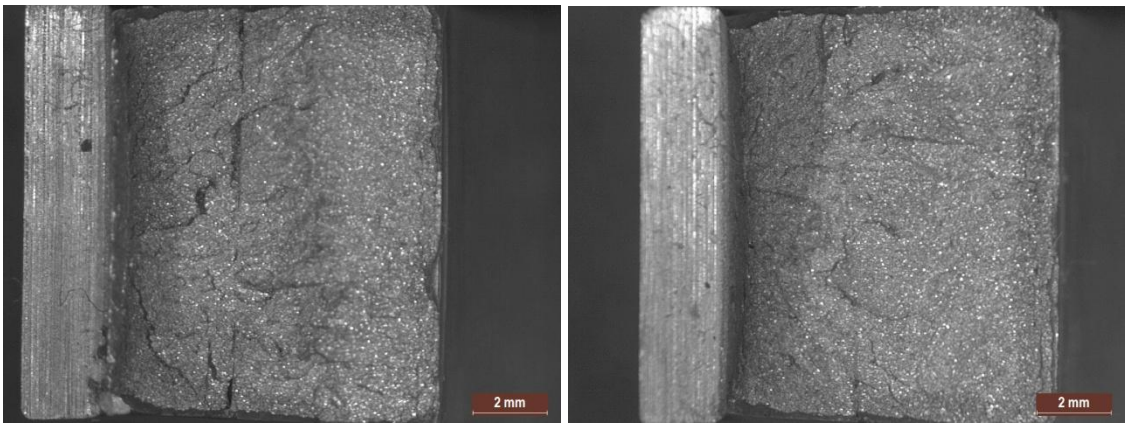

Figure 3.11 Brittle fracture of simulated samples-Peak Temperature of 957/1330 °C.

Chapter - 4

Conclusion and Future Scope

4.1 Conclusion

The weldability of Creep Strength Enhanced Ferritic/Martensitic (CSEF) steel T/P92 (9Cr2WV) was successfully executed with electrode Thermanit MTS616 from Böhler/Thyssen Schweiβtechnik, Germany using GTAW process from Kemppi machines at the optimised parameters low heat input parameters and the heat affected zone has been analysed with FEA modelling. The finales were:

1. The GTAW welding heat source model had been established based on SYSWELD numerical simulation and experimentally compared that has a variation of 25% high in simulated heat input than experimental heat input.
2. The microstructure and hardness comparison of simulated heat affected zone from double pass weld thermal cycle of sysweld and real time heat affected zone were found to have a variation of 15-10% at different regions. It can be fine-tuned towards correlation by experimentally measuring the thermal and mechanical properties of P92 steel at various temperatures and fine data acquisition systems. The extrapolated temperature dependent properties have to be further confined for accuracy so then it can be recommended for BHEL/IBR Standards.
3. The BM chemical composition and the welding thermal cycle's peak temperature had affected the real time microstructure of HAZs comprehensively. The coarser δ-ferrite are due to BM's retained thin δ-ferrite that nurtured quickly and cumulated at 1300 °C higher temperature in HAZs.
4. Mechanical Property of weld metal micro-hardness, tensile test, and root bend test had found to be in accordance with standards.
5. Transverse Face bend test reveals a crack of 5.2 mm in the matensitic HAZ region after a relaxation time of 24 hours.
6. Fracture toughness of weld metal by CVN technique was found to have energy variation of 2 J in comparison with British Standards BS EN 1599:1997 which can be increased by increasing preheat or with hot wire TIG process.

4.2 Future Scope:

1. Precise measurement or extrapolation of the values of thermal dependent properties with respect to temperature upto melting point has to be accomplished.
2. Real time thermal cycle has to measure by fine data acquisition thermocouple systems.
3. Oscillation during welding has to be taken into account for sysweld simulation.
4. Thermo mechanically simulated samples will be analysed for creep and tensile test to find allowable stress.

Reference

1. J.C. Vaillant, B. Vandenberghe, B. Hahn, H. Heuser, C. Jochum, Int. J. Press. Vessel Piping 85 (2008) 38.
2. M. Lomozikn, M. Zeman, J. Brozda, archives of Civil and Mech. Eng. 12 (2012) 49.
3. The T92/P92 book " Vallourec and Mannesmann tubes Page no: 11, 2010.
4. G.D. Janaki Ram, N.V. Ravi Kumar, K. Prasad Rao, project#RB/11-12/MET/004/BHEL/GDJA IIT Madras Met. And Mat. Eng., (2008).
5. C. Kocer, T. Abe, A. Soona, Mater. Sci. Eng. A 505 (2009) 1.
6. H. Zhang, B. Long, Y. Dai, J. Nuclear Materials 377 (2008) 122.
7. S. Prasad (2011), Simulation of precipitation in power plant steels. Project thesis. Dept. Met. and Mater. Eng., IIT Madras.
8. G. Vimalan, and G. Ravichandran J. WRI Vol.35 No.4 (2014) 5.
9. M. Consonni, 20889/05-3/12, TWI Ltd.
10. Properties of T/P92 steel weld metals for ultra super critical power plant by Z. Zhang, G. Holloway, A. Marshall, Metrode Products Limited, UK.
11. J. Onoro, Int. J. Press. Vessel Piping 83 (2006) 540.
12. J.D. Parker and G.C. Stratford, Strain localization in creep testing of samples with heterogeneous microstructures, Int. J. Press. Vessel Piping 68(1996) pp. 135.
13. K. Laha, K.S. Chandravathi, P. Parameswaran, K. Bhanu Sankara Rao and S.L. Mannan, Met. Mater. Trans.A, 38 (2007) 58.
14. Abe, Mater. Sci. and Eng. A 387–389 (2004) 565.
15. B. Kim, C. Jeong, B. Lim, Mater. Sci. Eng. A 483–484 (2008) 5.
16. B. Fournier, F. Dalle, M. Sauzay, J. Longour, M. Salvi, C. Caës, I. Tournié, P.F. Giroux, S.H. Kim, Mater. Sci. Eng. A 528 (2011) 6934.
17. S.T. Mandziej, Procedia Eng. 2 (2010) 349.
18. J. Goldak, A. Chakravarti, M. Bibby, 1984. Metall. Trans. B. 15, 299.
19. Complete finite element solution for simulation of welding process, J. Tejc, MECAS ESI s.r.o., CZ.
20. Y.Adonyi, Welding Journal, AWS (2006), 42.
21. W. Xue, S. Zhuan, P. Qian-gang, WU.Hong-liang, Trans. Nonferrous Met. Soc. China 19(2009) s772.
22. R. W. Niles and C. E. Jackson, Welding Research Supplement (1975) 25.

23. Shielding Gases Selection N Manual by Praxiar, Inc.
24. R. Scott Funderburk, Welding Innovation Vol. XV, No. 2, 1998.
25. L. Zhao, J. Liang, Q. Zhong, Advances in Eng. Software 68 (2014) 70.
26. Gleeble Users Training 2009, Gleeble systems and Applications by Dynamic Systems Inc.
27. L. Falat, A. Vyrostkova, V. Homolova, M. Svoboda, Engineering Failure Analysis 16 (2009) 2114.
28. G. Magudeeswaran, V. Balasubramanian, G. Madhusudhan Reddy, Defence Technology 10 (2014) 47.
29. B. Basu and K.K Sarkar, 3rd International Conference on Thermo-Mechanical Simulation and Processing of steels (2012) SAIL, Ranchi.
30. J. Wang, S. Lu, W. Dong, D. Li, L. Rong, Materials and Design 64 (2014) 550.